# Subtle and unexpected role of PEG in tuning the penetration mechanisms of PLA-based nano-formulations into intact and impaired skin

Augustine Lalloz, Marie-Alexandrine Bolzinger, Stephanie Briancon, Jimmy Faivre, Jean-Michel Rabanel, Araceli Garcia Ac, Patrice Hildgen, Xavier Banquy

# *Subtle and unexpected role of PEG in tuning the penetration mechanisms of PLA-based nano-formulations into intact and impaired skin.*

Augustine Lalloz[1,2], Marie-Alexandrine Bolzinger[2*], Stéphanie Briançon[2], Jimmy Faivre[1], Jean-Michel Rabanel[1,‡], Araceli Garcia Ac[1], Patrice Hildgen[1*], Xavier Banquy[1*]

[1]*Faculté de Pharmacie, Université de Montréal, C.P. 6128, Succursale Centre-ville, Montréal, Québec H3C 3J7, Canada*

[2]*Univ Lyon, Université Claude Bernard Lyon 1, CNRS, LAGEP UMR 5007, 43 Boulevard du 11 novembre 1918, F-69100, Villeurbanne, France*

[‡]*Present address : INRS-Institut Armand-Frappier, 531 Boulevard des Prairies, Laval, Québec H7V 1B7, Canada*

*Corresponding authors: xavier.banquy@umontreal.ca; patrice.hildgen@umontreal.ca

marie.bolzinger@univ-lyon1.fr

## Abstract

We present a systematic study of the role of poly(ethylene glycol) (PEG) content in NPs on drug skin absorption. Cholecalciferol-loaded NPs of 100 nm of diameter were prepared by flash nanoprecipitation from PLA-*b*-PEG copolymers of various PEG lengths. As PEG content increased in the polymer, we observed a transition from a frozen solid particle structure to a more dynamic particle structure. Skin absorption studies showed that polymer composition influenced drug penetration depending on skin condition (intact or impaired). In intact skin, highly PEGylated NPs achieved the best skin absorption, even if the penetration differences between the NPs were low. In impaired skin, on the contrary, non-PEGylated NPs (PLA NPs) promoted a strong drug deposition. Further investigations revealed that the strong drug accumulation from PLA NPs in impaired skin was mediated by aggregation and sedimentation of NPs due to the release of charged species from the skin. In contrast, the dynamic structure of highly PEGylated NPs promoted wetting of the surface and interactions with skin lipids, improving drug absorption in intact skin. Since

NPs structure and surface properties determine the drug penetration mechanisms at the NP-skin interface, this work highlights the importance of properly tuning NPs composition according to skin physiopathology.


## Keywords

Polymeric nanoparticles, poly(ethylene glycol), skin penetration, interactions, penetration mechanisms, cholecalciferol

## 1. Introduction

The dermal route for local skin delivery or systemic drug delivery has many advantages, such as easy, non-invasive administration, and avoidance of first pass metabolism, but poses challenges. If no particular formulation is developed, diffusion of drugs towards the viable layers of the skin and the systemic circulation is limited, and confined to drugs with very specific properties, such as medium lipophilicity, low size and high potency(Prausnitz and Langer, 2008). This formidable barrier function of the skin is notably achieved by the specific structure of the *stratum corneum*, the upper layer of the skin, made of dead keratinized cells embedded in a mixture of organized lipids assembled as "brick and mortar"(Elias, 1983). To counteract the barrier properties, several types of formulations offer the opportunity to modulate the skin drug penetration. Among them, nanoparticles (NPs) have gained great attention in skin delivery research due to their ability to formulate lipophilic drugs, to control the drug release, and to target specific skin layers and follicular pathway. The modulation of the drug penetration was found related to the nanocarrier type (liposomes, lipid particles, polymeric particles) and its physicochemical properties which influence the surface effects on the skin (interactions with lipids, film formation, occlusion) as well as drug release from the nanocarrier (Bolzinger et al., 2011; Papakostas et al., 2011). A strong accumulation of nanocarriers in the *stratum corneum* or their penetration in skin appendages also help drugs to overcome the skin barrier (Knorr et al., 2009), even if the penetration of the NPs themselves into the viable skin layers is uncertain and unlikely on intact skin (Baroli, 2010).

Nevertheless, the possible interactions between the skin components and the NPs which control the mechanisms of drug delivery are still unclear, as well as the role of the skin

physiopathology on these interactions. In fact, pharmaceutical skin formulations are mainly topical products intended to treat cutaneous diseases and therefore to be used on a non-intact skin characterized by an alteration of the cutaneous barrier function due to histological and skin microenvironment changes. For example, wounds, scratches, inflammation or alteration of the lipid composition and organization, as in the case of atopic dermatitis, are responsible for a damage of the skin barrier (Elias and Steinhoff, 2008). In other cases, disorders of the epidermal differentiation (psoriasis, ichthyosis, skin cancer…) are characterized by an epidermal thickening (Griffiths and Barker, 2007; Marukian and Choate, 2016), also altering the skin barrier properties. In addition, skin of premature newborn children is also characterized by a less efficient cutaneous barrier (Harpin and Rutter, 1983). Since skin penetration studies from NPs are in most cases performed on healthy skin models, the effect of the pathological condition of the skin is often underestimated when developing efficient nanocarriers for skin delivery. It is however a key effect to consider. In fact, it was notably found that the penetration profiles of drug in injured skin (abraded, stripped, inflamed, delipidated) was clearly different than from intact skin (Abdel-Mottaleb et al., 2012; Döge et al., 2016; Jensen et al., 2011; Tsai et al., 2001), as well as the fate of the nanoparticles in skin (Alnasif et al., 2014; Rancan et al., 2017), due to the damages of the *stratum corneum* which weaken the skin barrier function. Nonetheless, an increased skin penetration was not systematically reported (Alnasif et al., 2014; Boakye et al., 2015; Štecová et al., 2007), highlighting the importance to systematically study this effect.

Even though no general rules concerning skin drug penetration were defined so far, a lot of NPs characteristics have been reported to affect both drug and NPs skin penetration.

Among them, the physical properties of the NPs such as size (Shim et al., 2004; Vogt et al., 2006), and deformability (Cevc and Chopra, 2016; Honeywell-Nguyen et al., 2004) are well-known. Some evidences also recently demonstrated the influence of the NPs shape (Fernandes et al., 2015; Tak et al., 2015). Drug accumulation in the skin also depends on the composition of the NPs core, since the solubilizing properties of the encapsulating material towards the drug influence the partition coefficient of the drug from particles to the skin (Laredj-Bourezg et al., 2015). The surface properties are other important NPs characteristics which likely control skin NPs-interactions. A lot of studies have shown the influence of NPs surface charge on the skin penetration (Fernandes et al., 2015; Kohli and Alpar, 2004; Wu et al., 2010), even though conclusions were often contradictory. In fact, in addition to surface charge, other surface properties must also be considered, such as the composition. For example, the hydrophilic or hydrophobic composition of the particle surface is still a poorly systematically studied characteristic although it may also play a role in the mechanisms of drug penetration by dictating the type and intensity of NPs interactions with the skin surface and so the nanoparticle fate on skin. For example, a study by Rancan *et al*. showed that bare lipophilic PLA NPs loaded with a lipophilic fluorochrome tend to lose their particulate morphology after incubation on human skin surface (Rancan et al., 2012b). It was also been demonstrated that the surface functionalization of gold particles with a hydrophilic poly(ethylene glycol) (PEG) corona was beneficial to prevent their aggregation induced by skin (Mahmoud et al., 2016) and, to improve the deposition of particles in skin layers (Mahmoud et al., 2017) or in follicles (Hsiao et al., 2016). It is also likely that the interactions between skin and NPs surface strongly depend on the skin surface condition. In fact, on intact skin, NPs are deposited on

a non-viable lipophilic surface. On the contrary, if the *stratum corneum* is damaged, the interactions are expected to be drastically different since the particles may interfere directly with the more hydrophilic and viable suprabasal layers.

Recently, amphiphilic block copolymer particles which form a lipophilic core-hydrophilic surface structure, have demonstrated their potential for skin drug delivery compared to commercial formulations or to lipid nanoformulations (Bachhav et al., 2011; Kilfoyle et al., 2012; Lapteva et al., 2014; Laredj-Bourezg et al., 2015; Ramezanli et al., 2017; Shim et al., 2004). The use of this kind of particles to favour drug absorption in topical treatment seems to be an interesting strategy compare to bare lipophilic NPs in order to reduce NPs destabilization and to possibly interact more efficiently with the hydrophilic skin layers in case of damaged skin. Nonetheless, we recently observed the inverse trend since we showed that the presence of a hydrophilic coating of PEG or poly(2-methacryloyoxyethylphosphorylcholine) on PLA-based polymeric NPs significantly reduced absorption of cholecalciferol in damaged skin (stripped skin) compared to bare lipophilic PLA NPs (Lalloz et al., 2018). In addition to the hydrophilic or lipophilic nature of the skin, other parameters are therefore likely to affect the interactions of the NPs with the skin and so the drug absorption, depending of the NPs hydrophilic composition.

The objective of this systematic study was thus to understand more specifically the role of the hydrophilic polymeric content of PLA-based NPs on the penetration of cholecalciferol in both intact and impaired skin, *via* skin-NPs interactions studies. Cholecalciferol was chosen as a strong lipophilic model drug due to its chemical structure closely related to its active metabolite, calcitriol, which is a first-line treatment of psoriasis. Firstly, a library of cholecalciferol-loaded PLA based NPs with increasing PEG content in NPs was prepared.

PEG content in NPs was varied by using PLA-b-PEG polymer of different PEG lengths. The preparation process was tuned to obtain identically sized NPs regardless of the chemical composition of the polymer, in order to rule out potential size effects across all formulations. The physicochemical properties and structures of the NPs were fully characterized as a function of polymer composition. The NPs formulations were then systematically compared with regard to drug penetration into intact skin and into a model of barrier-disrupted skin. Special attention was paid to the examination of the interactions between NPs and skin components to gain insights into the mechanisms of drug skin penetration enhancement from polymeric NPs according to NPs hydrophilic composition.

## 2. Materials and Methods

### 2.1 Materials

Analytical grade acetonitrile, methanol and chloroform were purchased from Fisher Scientific (Loughborough, UK). Acetone was obtained from Biosolve Chimie (Dieuze, France). Dimethylformamide (DMF) was obtained from Prolabo (Paris, France). Solvents were used as received. Deionized water of 18 MΩ cm resistivity was used throughout the work. Cholecalciferol, deuterated chloroform, and deuterated water have been supplied by Sigma Aldrich (Steinheim, Germany). Butylhydroxytoluene (BHT) was a gift from Clariant (Frankfurt, Germany). Oleth-20 surfactant (Brij® O20) was bought from Croda (Cleveland, UK). Ceramide NP was a kindly gift from Evonik (Essen, Germany).

For the preparation of Hank's Balanced salt solution (HBSS), potassium chloride, sodium chloride and D-glucose anhydrous were purchased from Fisher Scientific (Loughborough, UK), potassium dihydrogenophosphate was obtained from Prolabo (Paris, France), sodium bicarbonate was purchased from Cooper (Melun, France) and di-sodium hydrogenophosphate dihydrate was purchased from Sigma Aldrich (Steinheim, Germany).

### 2.2 Formulations Preparation and Purification

Cholecalciferol-loaded polymeric nanoparticles were prepared from a library of PLA and PLA-*b*-PEG polymers with PEG of different lengths ranging from 1 to 10 kDa (PLA, PLA-*b*-PEG1K, PLA-*b*-PEG2K, PLA-*b*-PEG5K and PLA-*b*-PEG1K). The polymers were synthesized by ring opening polymerization and characterized in terms of molecular weight and $\%_{w/wtotal}$ of PEG in polymers, according to the protocols described in Supporting Information.

A typical procedure of nanoparticle fabrication using a Confined Impingement Jet (CIJ) Mixer (Flash Nanoprecipitation) is described below. The CIJ mixer was fabricated in house according to the blueprint of Han et al. (Han et al., 2012).

The organic phase was composed of 30 mg of PLA or 60 mg of PLA-*b*-PEG polymer (1 or 2 % $w/v_{organic\ phase}$), cholecalciferol (7% $w/w_{polymer}$ i.e. 0.07 or 0.14 % $w/v_{organic\ phase}$) and BHT (4 % $w/w_{polymer,}$ i.e. 0.04 or 0.08 % $w/v_{organic\ phase}$) dissolved in 3 mL of acetone. BHT was used to prevent cholecalciferol degradation. The organic solution was transferred in a 3mL syringe and a second syringe was loaded with 3 mL of distilled water. The two syringes were connected to the CIJ mixer and the two phases were injected into the mixing chamber at an equal flow rate by hand motion. In order to obtain NP of same size, the total flow rate was varied depending on the polymer. Immediately after mixing, the nanosuspension was diluted in 12 mL of distilled water stirred at 400 rpm to allow a rapid quenching.

To remove the organic solvent, the nanosuspensions were dialyzed against distilled water under stirring during 3h in a regenerated cellulose membrane bag with a cut-off of 10-12kDa (Spectra Por, Spectrum Laboratories, Rancho Dominguez USA). Then, organic solvent residuals were gently evaporated under reduced pressure. Finally, the nanosuspensions were purified by centrifugation at 2 300 g for 5 minutes to remove aggregates of polymers. The supernatant loaded in nanoparticles was collected (polymer yield > 85%).

## 2.3 Nanoparticles Characterization

### 2.3.1 Size measurements

The NP size was determined by dynamic light scattering (DLS) on a Malvern Zetasizer NanoSeries (Malvern, Worcester, U.K.) at a diffraction angle of 173°. Measurements were done in triplicate in deionized water.

### 2.3.2 Zeta potential measurements

The NP Zeta potential was determined by electrophoretic light scattering on a Malvern Zetasizer (Malvern, Worcester, U.K.). Measurements were done in triplicate after suspension of NPs in 5 mM NaCl solution.

### 2.3.3 Drug loading and drug yield

Cholecalciferol content in NPs suspensions after purification were determined by dissolving 100 µL of NP in 900 µL of acetonitrile. The solutions were then filtered through a 0.2 µm nylon membrane filter (Uptidisc®, 13 mm, Interchim, Montlucon, France) and analyzed by an UV-HPLC method described below (Material & Methods, paragraph 5). NPs concentration was determined by freeze-drying and accurate weighing 1mL of NPs suspension.

Percent drug loading and percent drug yield were calculated using equations (1) and (2) respectively.

$$Percent\ drug\ loading\ (\%) = \frac{weight\ of\ cholecalciferol\ in\ nanosuspension}{weight\ of\ NPs} * 100 \quad \text{Eq. 1}$$

$$Percent\ drug\ yield\ (\%) = \frac{weight\ of\ cholecalciferol\ in\ nanosuspension}{weight\ of\ cholecalciferol\ fed\ initially} * 100 \quad \text{Eq. 2}$$

### 2.3.4 Quantification of fabrication yield

In order to determine the amount of nanoparticles fabricated from the polymers, 5 mL of cholecalciferol/BHT loaded nanosuspensions were centrifuged (2 h at 50 000 g). The nanoparticle pellet and the supernatant obtained after centrifugation were freeze-dried and accurately weighed. The composition of the polymer in the supernatant was determined by $^1$H NMR (Varian 400-MR, Varian, USA). The fraction of free polymer chains/micelles remaining in suspensions and which did not form nanoparticles was calculated using the equation (3):

$$Percent\ free\ polymer\ chains\ (\%) = \frac{weight\ of\ polymer\ in\ supernatant}{weight\ of\ polymer\ and\ drug\ after\ purification} * 100$$

Eq. 3

### 2.3.5 Total and surface PEG quantification by NMR Analysis

NPs were first concentrated (up to 5-fold) by ultrafiltration (Ultrafiltration disk membranes, 10 kDa, 76 mm, Millipore®, Sigma Aldrich, Steinheim Germany)

To determine total PEG content in the NPs, 1 mL of the concentrated nanosuspension was freeze-dried in an Eppendorf tube, then dissolved in $CDCl_3$ with tetramethylsilane as internal standard and analyzed by $^1$H NMR (Bruker AV500, Bruker, Germany). The mass concentration of the NPs was also determined for PEG surface density calculations.

For surface PEG quantification, 500 µL of concentrated NPs suspension were added to 500 µL of deuterium oxide using DMF as an internal standard and analyzed by $^1$H NMR (Bruker AV500, Bruker, Germany). Quantifications were conducted with reference to the

internal standard peak intensity. PEG chain surface densities were calculated as previously described (Rabanel et al., 2015a).

#### 2.3.6 Cryo-Transmission Electron Microscopy (Cryo-TEM)

Drug-loaded NPs were imaged at the Centre de Caractérisation Microscopique des Matériaux ($CM^2$) technical facility of the Université de Montréal. 3 µL droplets of NP suspensions (0.1−1 mg/mL) were deposited on Formvar-Carbon 200 mesh copper grids (Canemco-Marivac, Lakefield, Canada) at room temperature for 10 minutes. After incubation, excess of suspension was soaked with a wiper and grids were air-dried for 2-3 hours before imaging. No staining procedure was used.

The microscope used for the acquisition is a JEM-2100F field-emission electron microscope (Jeol Ltd., Tokyo, Japan) operating 200 kV acceleration voltage. The grids were introduced into the microscope column under vacuum. The samples were cooled with liquid nitrogen added in the sample holder (Gatan Inc., Warrendale, PA). Image acquisition was performed in bright-field mode with a digital camera at low electron dose to prevent damage to the heat-sensitive particles. A temperature controller (Smart Set model 900 cold stage controller; Gatan Inc.,Warrendale, PA) maintained the grids at -150 °C during the imaging process.

#### 2.3.7 Colloidal Stability studies

The colloidal stability of all polymeric nanoparticles in aqueous suspensions was investigated by monitoring the hydrodynamic diameter and zeta potential of the particles stored at 4°C.

### 2.4 Skin Penetration Studies

### 2.4.1 Skin preparation

Porcine flank skin from 4 donors was used for the skin absorption studies. Skin was obtained from young female pigs freshly sacrificed at the École de Chirurgie (Université Claude Bernard Lyon-1, Lyon France). Skin was frozen at -20°C until use for a maximum of 3 months. On the day of experiments, skin was thawed at room temperature. Hairs were removed with an electric clipper. The subcutaneous fatty tissue was removed with a scalpel and the excised skin was cleaned up with tap water. Skin thickness was measured with a caliper (Mitutoyo) (1.25 ± 0.10 mm). Transepidermal water loss (TEWL) on each skin piece was determined using a Tewameter TM300 (Courage + Khazaka Electronic GmbH, Köln, Germany) to evaluate the skin integrity according to OECD guidelines (OECD). Skin pieces with a TEWL value higher than 15 $g.m^2.h^{-1}$ were discarded.

To highly impair skin barrier, SC was removed by tape stripping (Standard D-Squame, Monaderm, Monaco) up to reach a TEWL value between 30-40 $g.m^2.h^{-1}$ (Dey et al., 2014; Tsai et al., 2003).

### 2.4.2 In vitro assessment of cholecalciferol skin absorption

Cholecalciferol transport through skin from the nanosuspensions was assessed on Franz static diffusion cells. Skin pieces were mounted between the donor and receptor chambers of Franz cells (diffusion area = 2.54 $cm^2$, n > 7 independent experiments). The 10 mL receptor compartment was filled with HBSS buffer at pH 7.4 containing 0.5 % of oleth-20 to ensure sink conditions and 0.002 % of BHT to avoid drug oxidation. After 30 min of equilibration, 0.4 $mL/cm^2$ of freshly prepared polymeric formulations was deposited on the skin surface, which corresponds to a cholecalciferol deposition of 35 µg/cm² NPs were diluted if necessary to achieve a cholecalciferol concentration of 90 µg/mL in all

formulations (skin deposition of 35 µg/cm$^2$) and a polymer concentration of 1.2 mg/mL (skin deposition of 0.47 mg/cm$^2$). The receptor compartment was stirred at 400 rpm. All experiments were carried out under occlusive conditions and in a dark place for 24 h to avoid drug degradation. The water bath was maintained at 37°C to ensure 32±2°C at the surface of the skin. At the end of the study the receptor fluid was removed, and freeze-dried. Franz cells were dismantled. The skin surface was washed three times with 1 mL of a fresh receptor fluid solution and wiped with a cotton swab to recover the non-absorbed fraction. The skin surface was stripped once to remove the last residues of NPs adhering to the skin. For intact skin only, *stratum corneum* was removed by tape stripping (28 strips) (Standard D-Squame, Monaderm, Monaco). The viable epidermis and dermis were separated by heat treatment in water at 60 °C for 45 s and were cut into small pieces with a scalpel. Cholecalciferol was extracted from each fraction (skin layers, freeze dried receptor fluid and residual formulation) with acetonitrile containing 0.002 $\%_{w/w}$ BHT under ultrasounds for 1 hour. Samples were filtered through a 0.2 µm nylon membrane filter (Uptidisc®, 13 mm, Interchim, Montlucon, France) before analysis by an UV-HPLC method described below (Material & Methods, paragraph 5).

### 2.5 HPLC Titration of Cholecalciferol

Cholecalciferol content was analyzed using liquid chromatography with a reverse phase column using a previously published method with a slight modification (Almouazen et al., 2013). The HPLC set up from Waters (St Quentin en Yvelines, France) was composed of a Waters 717 injector, a Waters 600 pump, a reverse phase column XSelect® HSS C18 (4.6 × 150 mm, 3.5µm) and a Waters 2998 photodiode array UV detector working at 266 nm wavelength. The isocratic elution with methanol/acetonitrile (90:10) solvent at

1 mL $min^{-1}$ flow rate and 30 °C gave a retention time of 6.6 min for cholecalciferol. Injection volume was 20 or 40 µL. The calibration curve for quantitative analysis was from 20 to 0.03 $\mu g.mL^{-1}$. Data were analyzed with Empower 3 software.

## 2.6 Interactions Between Skin Components and Nanoparticles

### *2.6.1 NPs stability in suspension upon exposure to skin-conditioned solution*

Because the physical state of the NPs upon skin exposure may affect skin penetration (Labouta and Schneider, 2013; Rancan et al., 2012a), the colloidal stability of NPs due to species released from skin or present on skin surface was carefully studied. In brief, pieces of intact skin or damaged skin were mounted on Franz diffusion cells using the same protocol as used for the penetration studies in section "*In vitro assessment of cholecalciferol skin absorption"*. 0.4 $mL/cm^2$ of deionized water was deposited on skin. After 24 hours of incubation, the "skin-conditioned solutions" were filtered through 0.2 µm nylon membrane filter to remove skin debris and protein aggregates. The osmolarity of the conditioned-solutions was quantified with an osmometer (Micro-Osmette™, Precision Systems Inc, Natick, USA) and was considered as an estimation of the amount of soluble species released in the conditioned-solution.

In order to evaluate the NPs stability in the same conditions as during skin penetration studies (i.e. same concentration of NPs and same concentration of soluble species originating from skin), the filtrated "skin-conditioned solutions" were first concentrated. To concentrate, the filtrates were freeze-dried, and the dry residues were dissolved in a known smaller volume of deionized water. The concentrated "skin-conditioned solutions" were then diluted with NP suspensions to reach skin penetration concentrations of NPs (1.2

mg/mL) and soluble species. The stability of the NPs was evaluated after mixing with the "skin-conditioned solutions" by monitoring NPs size for 24 hours by DLS. For each condition (intact or stripped skin), tests were replicated with n=6 skin pieces from 6 different pigs.

### *2.6.2 Visualization of NPs sedimentation on impaired skin surface*

0.4 mL/cm$^2$ of fluorescent NPs (diluted at 1.2 mg/mL) made of a mixture of PLA / PLA-Cy5 (90/10 %w/w) or PLA-*b*-PEG1K/PLA-Cy5 (90/10 %w/w) was deposited onto stripped skin pieces mounted in Franz cell according to the same protocol than described in section "*In vitro assessment of cholecalciferol skin absorption"*. After 24h of incubation, residual formulation was removed, and skin pieces were wiped with a cotton swab. One tape strip was performed to remove the formulation residues adhering/sticking to the skin. Skin strip was deposited on a microscopy slice and imaged using an Olympus IX81 microscope equipped with a Olympus UPlanSApo 10×/0.40 Infinity/0.17 FN26.5 objective (Olympus Canada Inc., Toronto, ON,Canada), a 12 bits Retiga-2000R CCD Camera (QImaging, Surrey, BC, Canada) and MetaMorph® Advanced software. The mean fluorescence intensities of the images were calculated using ImageJ software (Image J. U. S. National Institutes of Health, Bethesda, Maryland, USA.). Tests were replicated with n = 5 skin pieces from 3 different pigs. Three images at least were taken per strip.

### *2.6.3 Evaluation of the alteration of lipid surface model*

Ceramides NP coatings on cleaved mica slides were performed at room temperature with a built-in house spin coater. This ceramide type is the most abundant in the stratum corneum intercellular lipid matrix. 40 µL of ceramide NP in chloroform (0.5 mg/mL) were

spin coated on mica sheets of 1cm diameter at 1000 rpm for 30 seconds. After coating, the lipid films were air-dried for 2 hours. The contact angles of a water droplet (10 µL) on the lipid surfaces were then measured with a contact angle meter (Tantec, Model CAM Micros, Schaumburg, USA) before and after 24h of incubation at 32ºC in 1mL of nanosupensions (diluted at 1.2 mg/mL). All contact angles were determined at room temperature. Three replicated experiments were performed for each nanosuspension. The work of adhesion $W_{LS}$ was calculated from the contact angle data using the Young-Dupré equation (equation 4):

$$W_{LS} = \sigma_{LV}(1 + cos\theta) \quad \text{Eq. 4}$$

where $W_{LS}$ is the work of adhesion liquid-solid, $\sigma_{LV}$ the interfacial tension liquid-vapor and $\theta$ the contact angle.

### 2.7 Data analysis

Statistical analysis of differences between two groups were analyzed by Student t-test and those between multiple groups were performed using the analysis of variance (ANOVA, one-way) followed when needed by LSD t-test. The significance level (p) was set at 0.05.

# 3. Results and Discussion

## 3.1 Increase of PEG chain length induces structural changes from solid NPs to micellar NPs

The NPs were fabricated from PLA or PLA-*b*-PEG copolymers synthesized by ring opening polymerization. PLA-*b*-PEG copolymers exhibited a PLA block in the range of $M_w$ 14 to 25 kDa and a PEG block of $M_w$ ranging from 1 to 10 kDa with narrow polydispersity index (PdI). PLA and fluorescent PLA homopolymers have a lipophilic block of 36 kDa. The PEG content in the polymers measured by NMR varied from 0 to 24.9% w/w. Mass molecular weight, $M_w$, polydispersity index, and PEG content are presented in Table 1.

Since particle size is a factor known to control drug penetration into skin (Alvarez-Roman et al., 2004; Patzelt et al., 2011; Shim et al., 2004), NPs with identical hydrodynamic diameter were produced and used throughout the study. To obtain NPs of identical hydrodynamic size, the flow rate used during Flash Nanoprecipitation (FN) was tuned according to the PEG weight content in the polymer. Indeed, it has been reported that NPs size made of diblock copolymers depends heavily on the weight ratio of the hydrophobic/hydrophilic blocks (Lalloz et al., 2018; Rabanel et al., 2015a) and can be modulated by varying the flow rate of each injected phase (Han et al., 2012; Johnson and Prud'homme, 2003; Lalloz et al., 2018; Shen et al., 2011). As measured by DLS, NPs with a hydrodynamic diameter $D_H$ = 100 nm (PdI < 0.1) were successfully obtained regardless the polymer used (Table 2).

The surface properties of the NPs, i.e. the zeta potential and the surface PEG content, were measured as a function of the total PEG content in the polymers. The surface density of PEG increased from 0 to 48 ethylene oxide units per $nm^2$ with the total PEG content in the

polymer (Table 2). Along with the increase of PEG content on NPs surface, a decrease of the ZP from -33 to -3 mV was observed as expected due to shielding of the NP surface charges by the PEG layer.(Gref et al., 1999)

The morphology of the NPs was imaged by cryo-TEM. Samples were cryogenized to prevent the collapse and deformation of the NPs during imaging. All particles presented a round-shaped morphology (Figure 1A). However, clear differences of particle structure were observed depending on the quantity of PEG in the polymers. For polymers with 8 %w/w of PEG or less (Figure 1A), only solid core nanoparticles were observed while for higher PEG contents (> 24 %w/w), a background of loosely aggregated polymer chains was systematically observed.

These first observations suggested a marked difference in structure between low and highly PEGylated NPs. The evolution of NPs size over time was then investigated to corroborate these first results (Figure 1B). Once again, when PEG content was 8 %w/w or lower, the size of the NPs was stable at 4°C varying less than 10 nm over 3 months. Oppositely, at higher PEG content, a continuous increase of the NPs size with time, ranging from 100 nm to 143 nm, was noticed. The ZP was however found to be stable over the same period of time (Figure S4, SI) for all polymers, indicating that no significant change of the NP surface properties such as PEG degrafting from the NP surface has occurred.

To gain more insights into the destabilization mechanism occurring for the highly PEGylated NPs, we quantified the amount of free polymer in each nanosuspension. Indeed, considering the wide range of hydrophobic (PLA) / hydrophilic (PEG) block length ratio of the PLA-*b*-PEG copolymers, we can anticipate that a substantial fraction of the most hydrophilic copolymers might remain soluble in water in equilibrium with the NPs. The

fraction of polymer forming particles and the fraction remaining as free chains in solution were therefore recovered after ultracentrifugation, in the pellet and supernatant respectively. As showed in Figure 1C, in nanosuspensions produced with 8 %w/w of PEG or less (PLA, PLA-b-PEG1K and PLA-b-PEG2K NPs), only a small fraction of polymer did not form aggregates and remained as free chains (< 7 %w/w). In contrast, when the PEG content in the polymer was superior to 8 %w/w (PLA-b-PEG5K and PLA-b-PEG10K NPs), a significant fraction of free polymer chains in the supernatant could be observed. In these nanosuspensions, the block-copolymer existed in the form of (1) 85 %w/w aggregates and (2) 15 %w/w single polymer chains. The PEG content in the fraction of free polymer chains was significantly higher compared to bulk polymer (63 vs 25 %w/w) explaining their propensity to stay in their unimolecular form. The presence of both aggregates and PLA-*b*-PEG free chains suggests a greater mobility of these chains in the dispersion medium and therefore faster NPs - medium exchange rates. Such high mobility should promote Ostwald ripening of the NPs and therefore mediate their observed instability.(Wooster et al., 2008) The Ostwald ripening rate, $k$, was quantified using Equation. 5 (Lifshitz-Slyozov-Wagner theory (Lifshitz and Slyozov, 1961; Wagner, 1961)) from the size stability data:

$$R^3 - R_0^3 = kt \qquad \text{Eq.5}$$

where $R$ and $R_0$ are the hydrodynamic radii of the particle at time $t$ and $t = 0$, respectively.

It was found that $k$ drastically increased for highly PEGylated NPs and correlated well with the fraction of free polymer chains in nanosuspension (Figure 1C). This observation confirmed that a significant Ostwald ripening occurred for these highly PEGylated NPs.

Two different structures were therefore detected depending on the PEG content in polymer. Nanoparticles produced from polymers with low or no PEG content (PLA, PLA-b-PEG1K, PLA-b-PEG2K) exhibit a "solid" or "frozen" behavior (low free polymer content, long term colloidal stability in pure water) whereas highly PEGylated nanoparticles (PLA-b-PEG5K and PLA-b-PEG10K) presented a more dynamic structure similar to polymeric micelles (high free polymer content, low colloidal stability). Interestingly, the present data tend to demonstrate that the transition from solid-like to micelle-like particles with polymer composition is abrupt and similar to already reported data for comb-polymers.(Rabanel et al., 2015a)

However, these differences in structure did not affect the encapsulation of the active compound due to the strong lipophilic character of the latter (logP = 7.5). Drug loading and drug yield were found independent of the polymer composition (Table 2). In addition, DSC analysis was performed to identify the physical state of the drug according to the polymer used. No fusion peak appeared in the DSC thermograms suggesting that cholecalciferol is present in an amorphous state in all the suspensions (Figure S5, SI).

### 3.2 Skin penetration of encapsulated active compound is PEG-dependent

Skin penetration of cholecalciferol was performed to evaluate the influence of copolymer composition and NPs structure on the delivery of a lipophilic drug to the skin. It was verified beforehand that less than 10% of cholecalciferol degradation occurred when the formulations are incubated in the conditions of skin penetration tests (37°C in a dark place for 24 hours) (Figure S6, SI). Porcine skin was used as the most relevant animal model because of its high structural similarities with human skin (Simon and Maibach, 2000). Penetration in both intact and stripped (impaired) skins was investigated to elucidate the

role of the skin condition on NPs / skin interactions. Stripped skin was chosen as a basic model for skin presenting impairment of the skin barrier as is the case in some skin pathologies (scratches, diseases, sunburns...). The tape-stripping method allows a highly homogeneous and effective removal of the *stratum corneum* with no substantial alteration of the viable epidermis (Döge et al., 2017). On intact skin, NPs were in direct contact with the *stratum corneum*, which is a lipophilic and dense layer of dead cells. On the contrary, on stripped skin, NPs were in contact with the viable epidermis surface, which is a porous and hydrophilic layer of living cells.

The amount of cholecalciferol in skin and its distribution throughout the skin layers after 24 hours exposure to the NPs formulations are presented in Figure 2, Figure 3 and Table 3. The results clearly showed that the amount of PEG in the formulation modulated the total cholecalciferol absorption in impaired and to a lesser extent in intact skin.

In intact skin and independently of the NPs formulation, cholecalciferol was poorly absorbed (less than 300 ng/cm$^2$, i.e. less than 1% of the applied dose) (Figure 2A and Table 3) and accumulated significantly in the *stratum corneum* (up to 200 ng/cm$^2$) and, to a lesser extent, in the viable epidermis (up to 100 ng/cm$^2$) (Table 3). Drug absorption in dermis was limited (less than 25 ng/cm$^2$) and none of the NPs formulations allowed a quantifiable permeation of the active compound in the receptor medium (Table 3). Such very low absorption in intact skin is commonly reported for this drug (Alsaqr et al., 2015; Ramezanli et al., 2017) and the affinity of cholecalciferol to the lipophilic layer of the *stratum corneum* was expected due to the strong hydrophobic character of the drug. Theses observations were also in line with other reports which showed that polymeric NPs favored the epidermis storage of lipophilic drugs while limiting their permeation in receptor compartment (Balzus

et al., 2017; Laredj-Bourezg et al., 2015). As mentioned, NPs composition had only a slight influence on the total drug absorption into intact skin. Small but significant differences were however found between low and high PEG content NPs formulations. The highest total absorptions of cholecalciferol in skin were observed for high PEG content NPs (PLA-b-PEG5K NPs: 0.29 µg/cm$^2$ and PLA-b-PEG10K NPs: 0.30 µg/cm$^2$) while the lowest absorption was measured for low PEG content NPs (PLA-b-PEG1K NPs: 0.20 µg/cm$^2$ and PLA-b-PEG2K NPs: 0.19 µg/cm$^2$) (Figure 2A). PLA NPs allowed a medium skin penetration, but which was not significantly different from PEGylated NPs. The distribution in the skin layers followed the same trends as the total amount absorbed in skin (Table 3).

On stripped skin, the total active compound absorption was significantly increased compared to intact skin for all tested formulations (from 0.3 to 0.8 µg.cm$^{-2}$) (Figures 2C and Figure 3), as expected due to the impairment of the barrier function (Boakye et al., 2015; Contri et al., 2016; Jensen et al., 2011; Rancan et al., 2017b). The penetration was enhanced in all viable layers of the skin but remained negligible in the receptor compartment (<0.02% of the dose) (Table 3). Such particles are therefore favorable for topical treatment of skin diseases since, even in impaired skin, they exhibited the highest skin penetration associated with the lowest permeation, allowing therefore to maximize drug efficacy while limiting adverse events (Boisgard et al., 2017). As for intact skin, when considering the PEGylated nanoformulations only, we can also notice that the increase in PEG content in the polymer (from 3.1 to 24.9 %w/w) resulted in a marked increase in drug penetration into stripped skin, ranging from 0.33 to 0.56 µg/cm2 (Figure 2B and Figure 3). A better accumulation in viable epidermis was notably achieved as the PEG content in NPs

increased (Table 3). This penetration increase seems controlled by the PEG content only and not by the PEG chain length since results obtained with PLA-b-PEG5K (24.9% w/w) and PLA-b-PEG10K (24.5% w/w) were identical (Figure 3). However, and contrary to intact skin, cholecalciferol loaded in PLA NPs displayed a significantly higher absorption in impaired skin compared to all the other NPs formulations ($p<0.05$) (Figure 2B and Figure 3) due to a better accumulation in both viable epidermis and dermis (Table 3). Notably, a 2.5-fold difference in drug penetration was found between PLA NPs and PLA-b-PEG1K NPs, which was significantly more pronounced compared to intact skin (1.2-fold). Moreover, the variation of drug penetration from intact to impaired skin was the most important for PLA NPs (+ 247 %) and the least important for PLA-b-PEG1K NPs (+ 72%) (Figure 2C), indicating that the impairment of the barrier function displayed various influences on drug absorption according to the NPs composition.

In the light of these results, different trends appeared according to NPs hydrophilic composition. In intact skin, the best cholecalciferol absorption was achieved by NPs having the most hydrophilic surfaces (PLA-b-PEG5000 or PLA-b-PEG10000 NPs), even if the differences of penetration between the different NPs formulations were low. In impaired skin, on the contrary, non-PEGylated NPs (PLA NPs) promoted a strong drug deposition. An increasing penetration of the drug was however also found as PEG content increased but was systematically lower than the cholecalciferol amount quantified for PLA NPs. We therefore hypothesized that such differences should arise from different interaction mechanisms of the NPs with the skin layers.

First, an increase of PEG surface coverage at the NPs surface enhanced the penetration of encapsulated cholecalciferol from PEGylated NPs, both in intact and impaired skin. On

impaired skin, nanocarriers are deposited on a hydrophilic structure (viable epidermis). The interactions between hydrophilic highly PEGylated NPs and skin surface seems therefore favored, allowing a better penetration of the drug compared to low PEGylated NPs. On the contrary, on intact skin, these results are at first sight unexpected considering the lipophilicity of the stratum corneum and the high surface hydrophilicity of the highly PEGylated NPs (PLA-b-PEG5K and PLA-b-PEG10K). However, different hypothesis may explain these results independently of the hydrophilic/lipophilic balance. First, we have shown that PEGylated particles can have a structure of solid NPs or micelle-like particles depending on their PEG content (Figure 1). As a consequence, the structure of highly PEGylated NPs is more dynamic, and free polymer concentration is significantly higher than weakly PEGylated NPs. These two factors are expected to play an important role in drug penetration. In fact, Deng et al. proposed that the deposition of micellar polymeric formulation onto skin provides a better wetting of the skin surface, making the drug carrier readily accessible to the skin (Deng et al., 2017). Free highly PEGylated chains in suspensions may also act similarly to permeation enhancers. Conte et al. suggested that PEG brush affected the organization of lamellar phase in the intercellular spaces of the *stratum corneum* (Conte et al., 2015), which could favor drug penetration. In addition, due to their loosely aggregated dynamic structure, it is possible that highly PEGylated NPs may undergo restructuring in skin through possible molecular dynamic reorganization. Such possible reorganization in skin may allow them penetrating deeper in the intercellular spaces of the skin favoring therefore the penetration of the drug.

Non-PEGylated NPs (PLA NPs) exhibited also unexpected trend since they demonstrated the highest drug absorption into impaired skin amongst all the formulations tested. This

trend is curious since these particles are hydrophobic and negatively charged, which may disfavor their affinities with the hydrophilic and negatively surface of impaired skin. It was however already reported that PLA nanoparticles formed aggregates after exposure to human skin explants (Rancan et al., 2009; Rancan et al., 2012b). Such a destabilization may enhance the release of the drug in the skin.

In order to understand more precisely the differences in drug penetration as a function of PEG content in PLA-based NPs formulations and skin condition, interactions between NPs and some skin components were characterized.

### 3.3 Colloidal stability and aggregates adhesion drive the penetration of encapsulated active compounds in non- and weakly PEGylated particles

A first key point to understand NPs interaction with skin components is to precisely assess the NPs stability once in contact with the skin surface. As recently pointed out by Mahmoud *et al* (Mahmoud et al., 2016), this parameter is usually underestimated when interpreting skin penetration results even though NPs instabilities may alter the biological effects of the NPs (Moore et al., 2015; Rancan et al., 2012a; Soenen et al., 2015). Therefore, the stability of the NPs suspensions in filtered aqueous solutions previously exposed to intact or damaged skin for 24 hours was assessed by DLS. These tests allowed quantifying NPs stability in presence of soluble species such as ions potentially released from skin into the suspension medium.

When immersed in a solution which was conditioned 24 hours with intact skin, all polymeric NPs suspensions showed no variation in hydrodynamic size which indicates excellent colloidal stability (Figure 4). In contrast, when exposed to solutions conditioned

with impaired skin, PLA and PLA-*b*-PEG1K NPs were rapidly destabilized. NPs with higher PEG content maintained their size over long period of time (24 h at least) indicating robust colloidal stability mostly imparted by steric repulsion between the NPs (Figure 4). These observations of skin induced aggregation depending of the NPs surface chemistry supported the study of Mahmoud *et al*. which also reported that the skin-induced destabilization of cationic gold nanorods was prevented by the presence of a PEG layer on their surface, providing steric stabilization (Mahmoud et al., 2016).

Among all the soluble species released from skin that could potentially destabilize the NPs suspensions, ions are certainly the most abundant ones. Indeed, solutions deposited on impaired skin were in direct contact with the viable epidermis, a layer which contains high level of salt species (Paweloszek et al., 2016) susceptible to be rapidly released. To confirm this assumption, we measured the osmotic concentration of solutions exposed to intact and stripped skin and compared these values to the critical coagulation concentration (CCC) of each type of NPs measured using NaCl as destabilizing salt. The CCC is the minimal concentration of salt leading to a rapid aggregation of particles (Rabanel et al., 2015a).. As shown in Figure S7 (SI), for PLA and PLA-*b*-PEG1K NPs, CCC was 17 and 40 mM respectively (34 and 80 mOsm/L respectively). Such aggregations arise from a diminution of the electrostatic repulsions between these NPs due to a neutralisation of their surface charges by saline species. In fact, these NPs are negatively charged as demonstrated by their Zeta potential values (-33 and -23 mV respectively). NPs with higher PEG content were found to be stable even in presence of a high concentration of salt (CCC > 2 M NaCl) due to the dense steric layer of PEG chains on the NP surface, as previously reported (Rabanel et al., 2015b). These observations were in excellent agreement with osmotic

concentration measurements of solutions exposed to skin surface. Osmolarity values measured on impaired skin were significantly higher (116 ± 41 mOsm/L) compared to intact skin (48 ± 52 mOsm/L) as expected. Since osmotic concentration values obtained from impaired skin were significantly higher than the values of the osmotic concentration at the CCC of PLA and PLA-*b*-PEG1K NPs, these NPs aggregated. These observations demonstrated that ionic species released from impaired skin trigger rapid aggregation of weakly PEGylated NPs in suspension when deposited on skin and therefore may accelerate their sedimentation onto skin surface. On the contrary, due to the dense PEG layer on their surface, PLA-*b*-PEG2K PLA-*b*-PEG5K PLA-*b*-PEG10K were stable in suspension when deposited on impaired skin.

Nonetheless, NPs aggregation only does not explain the drug penetration results reported in Figure 2. Indeed, non-PEGylated PLA NPs presented a 2.3-fold higher absorption of cholecalciferol in impaired skin compared to PLA-*b*-PEG1K NPs (Figures 2 and 3), even though both types of formulation are expected to form aggregates when in contact to impaired skin. Drug penetration appears therefore to rather depend on the adhesion of these aggregates to the skin surface.

To confirm this hypothesis, the affinity of the aggregates to the surface of impaired skin was investigated by analyzing the first adhesive tape strip usually performed to remove the last residues of formulation onto skin surface. A strong accumulation of drug from PLA NPs (0.44 ± 0.11 µg/cm$^2$) on damaged skin was found on the tape strip. In contrast, such accumulation was not observed for all the other NPs (< 0.08 µg/cm$^2$) (Figure 5A) even for highly PEGylated NPs which have also shown high cholecalciferol penetration (Figures 2 and 3). In addition, such strong accumulation of cholecalciferol was also not observed on

intact skin, tested as control (Figure 5A). To determine if strong drug accumulation on impaired skin from PLA aggregates stemmed from a drug release process from aggregates in solution or from sedimentation of the NPs on the skin surface, we repeated the experiment with PLA and PLA-*b*-PEG1K NPs covalently labelled with fluorescent dye cyanine 5 (Cy5) and measured the mean fluorescence intensity on the first strip. The average mean fluorescence intensity of three experiments was 807 ± 526 a.u for PLA NPs and 243 ± 399 a.u for PLA-*b*-PEG1K NPs (Figure 5B) confirming the significant deposition and adhesion of PLA aggregates on the first strip. In addition, we confirmed by fluorescence microscopy that both PLA and PLA-*b*-PEG1K NPs were indeed unstable and formed aggregates upon incubation with stripped skin (Figure 5C). However, a stronger build-up of micron-sized PLA NPs aggregates was clearly observed on the strips but were absent for PLA-b-PEG1K NPs (Figure 5C). These observations showed that PLA-*b*-PEG1K NPs formed aggregates when deposited on impaired skin but they staid in suspension and did not adhere to the skin surface, conversely to PLA aggregates. As shown in Figure 5A and B, the correlation between NPs adherence and drug accumulation at skin surface test is very strong, confirming that interactions between NPs and skin surface play an important role in the drug penetration. The strong penetration of the drug from PLA NPs in impaired skin is therefore the result of the strong adhesion of NPs aggregates formed *in situ* upon exposure to released ions. In fact, such an aggregates adhesion favored the aggregates contact to the outer skin surface and was therefore responsible for a higher local concentration of drug on skin surface, promoting its absorption. Moreover, it is likely that the preferential contact of the aggregates to the skin surface due to their

adhesion/sedimentation promoted indirectly the release of the drug from the polymeric carrier into the skin layers.

### 3.4 Affinity between highly PEGylated NPs and skin surface lipids mediate active compound penetration

Since highly PEGylated particles do not suffer from salt-induced colloidal aggregation, their capacity to increase drug penetration with the PEG content must be the result of their dynamic amphiphilic structure and free polymer presence. These two factors are expected to play an important role in the resulting affinity of the NPs with the skin surface, and especially with skin lipids.

We first try to detect any changes in the lipid organization of intact skin samples after exposure to the different nanoformulations using FTIR (Covi-Schwarz et al., 2017; Hasanovic et al., 2011). We found that the nanosupensions were too diluted (1.2mg/mL of NPs), to be able to cause any significant changes in skin structure. At this concentration, even sodium dodecyl sulfate did not induce any detectable alterations of lipid organization (data not shown). We therefore used a mica surface coated with ceramides to mimic the skin surface and characterize its interaction with the different nanosuspensions by measuring the Liquid/Solid work of adhesion, $W_{LS}$, before and after 24 h of treatment with the NPs. As shown in Figure 6, treatment with pure water had no effect on the interfacial properties of the ceramide film since the difference in work of adhesion before and after treatment was close to zero. A substantial difference of work of adhesion before and after the treatment was observable only for highly PEGylated NPs (-13 mN/m for PLA-b-PEG5K NPs and -17 mN/m for PLA-b-PEG10K NPs). The variation of work of adhesion was significantly smaller for weakly PEGylated NPs (< 5 mN/m). These results indicate a strong change in surface hydrophobicity only after treatment with highly PEGylated NPs

suspensions. These interfacial changes are the concomitant result of ceramide dissolution into the NPs suspension (an effect similar to detergency) and the adsorption of micelle-like aggregates and free polymer chains on the ceramides film.

Thanks to their dynamic structure allowing i) a better wetting of the skin surface and ii) a possible alteration of the lipid packing in the skin and which counteracted the unfavorable interactions with the lipophilic *stratum corneum*, the micelle-like highly PEGylated NPs promote the skin penetration of the drug in intact skin compared to the solid weakly PEGylated NPs. Such observations were in line with Deng *et al*. conclusions, who showed that Y-shaped PEG-$PCL_2$ micelles significantly disturbed the skin barrier (Deng et al., 2017). As previously hypothesized (Lapteva et al., 2014), we can also expect that highly PEGylated micelle-like NPs disassembled upon contact with the skin and diffuse in their molecular state, as liposome does (El Maghraby et al., 2006). An experimental evidence of the disaggregation tendency of the micelle-like NPs was provided by mixing the NPs and oleth-20 surfactant (Figure S8, SI). We observed a complete disassembly of micelle-like NPs in presence of surfactant. On the contrary, the solid NPs remained stable and were insensitive to the presence of the surfactant.

**3.5 Summary of the mechanisms**

The present study provides mechanistic insights on the interactions between NPs and skin layers.

In intact skin, we showed that cholecalciferol penetration only slightly depends of the NPs PEG content. The penetration of the active compound was therefore mostly controlled by its release rate from the NPs and by the affinity of the active compound to the different skin layers. The micelle-like structure of highly PEGylated NPs and the presence of free

polymer chains in the medium, facilitated nonetheless the wetting of the skin surface, favoring therefore the penetration of the encapsulated compound compared to weakly PEGylated NPs. A possible disaggregation of highly PEGylated NPs into the skin may also occurr.

In impaired skin, the role of NPs composition on the penetration of the active compound was much more pronounced. In addition to a weaker barrier function which favor drug skin penetration, impairment of the *stratum corneum* triggered the release of ionic species able to destabilize non- or poorly PEGylated particles. The sedimentation and the adhesion of the non-PEGylated aggregates favored therefore a strong accumulation of the drug on the skin-medium interface. Adhesion of NPs aggregates with impaired skin surface was however significantly weaker for poorly PEGylated particles, due to a reminiscent effect of the antifouling properties of grafted PEG chains. Hydrophilic highly PEGylated particles, which resisted skin colloidal aggregation, are likely to promote drug penetration via preferential affinities with the hydrophilic layer of viable epidermis. The hydrophilic dynamic structure was nonetheless less effective than NPs aggregation/adhesion mechanism in facilitating lipophilic drug penetration in impaired skin.

The possible skin penetration of intact NPs notably when in contact with impaired skin, their disassembly, as well as the impact of drug release process needs however further investigations.

## 4. Conclusion

The present analysis indicates that delivery of a highly lipophilic active compound to the skin via NPs encapsulation involves extremely subtle mechanisms of skin interactions, the prevalence of which depends on the NPs composition and on the physical state of the skin.

The salt-triggered mechanism of aggregation/sedimentation highlighted in this study seems therefore particularly interesting to increase the selectivity of formulation for patients whose physiological skin condition may not be uniform. In fact, even if formulation is spread on an area composed of intact and impaired skin, PLA NPs will only aggregate and sediment on impaired skin. In this way, the drug absorption will be only favored on impaired skin. Drug absorption in intact skin will be limited, which is expected to reduce adverse effects. This last conclusion suggests an interesting avenue to design drug delivery systems able to efficiently tune their penetration capacity accordingly to the pathological state of the skin. This last conclusion suggests an interesting avenue to design drug delivery systems able to efficiently tune their penetration capacity accordingly to the pathological state of the skin.

## Supporting Information

Polymer synthesis and characterizations protocols, Zeta potential stability studies, DSC analysis, drug degradation studies, NPs colloidal stability in saline and surfactant medium, can be found in Supporting Information available at ….

## Acknowledgments

AL is grateful to the Faculty of Pharmacy of Université de Montréal for their financial support and to the Région Auvergne-Rhône-Alpes for their mobility grant (Explo'RA Doc) and. JF is grateful to the Arthritis Society and the University of Montreal for PhD grants. AGA is supported by the TransMEdTech Institute. PH is thankful for the financial support of FRQNT. XB acknowledges the financial support from the Canada Research Chair Program and NSERC.

Technical assistance of Victor Badescu in polymer synthesis and NPs optimisation is acknowledged. Alexandre Melkoumov is acknowledged for the synthesis of the fluorophore Cy5-COOH. TEM imaging was performed with the help of Jean-Philippe Massé. Authors declare no competing interest.

# References


Abdel-Mottaleb, M.M., Moulari, B., Beduneau, A., Pellequer, Y., Lamprecht, A., 2012. Surface-charge-dependent nanoparticles accumulation in inflamed skin. J. Pharm. Sci. 101, 4231-4239.

Almouazen, E., Bourgeois, S., Jordheim, L.P., Fessi, H., Briançon, S., 2013. Nano-encapsulation of vitamin D3 active metabolites for application in chemotherapy: formulation study and in vitro evaluation. Pharm. Res. 30, 1137-1146.

Alnasif, N., Zoschke, C., Fleige, E., Brodwolf, R., Boreham, A., Rühl, E., Eckl, K.-M., Merk, H.-F., Hennies, H.C., Alexiev, U., Haag, R., Küchler, S., Schäfer-Korting, M., 2014. Penetration of normal, damaged and diseased skin — An in vitro study on dendritic core–multishell nanotransporters. J. Controlled Release 185, 45-50.

Alsaqr, A., Rasoully, M., Musteata, F.M., 2015. Investigating Transdermal Delivery of Vitamin D3. AAPS PharmSciTech, 1-10.

Alvarez-Roman, R., Naik, A., Kalia, Y.N., Guy, R.H., Fessi, H., 2004. Skin penetration and distribution of polymeric nanoparticles. J. Controlled Release 99, 53-62.

Bachhav, Y., Mondon, K., Kalia, Y., Gurny, R., Möller, M., 2011. Novel micelle formulations to increase cutaneous bioavailability of azole antifungals. J.Controlled Release 153, 126-132.

Balzus, B., Sahle, F.F., Hönzke, S., Gerecke, C., Schumacher, F., Hedtrich, S., Kleuser, B., Bodmeier, R., 2017. Formulation and ex vivo evaluation of polymeric nanoparticles for controlled delivery of corticosteroids to the skin and the corneal epithelium. Eur. J. Pharm. Biopharm. 115, 122-130.

Baroli, B., 2010. Penetration of nanoparticles and nanomaterials in the skin: fiction or reality? J. Pharm. Sci. 99, 21-50.

Boakye, C.H.A., Patel, K., Singh, M., 2015. Doxorubicin liposomes as an investigative model to study the skin permeation of nanocarriers. Int. J. Pharm. 489, 106-116.

Bolzinger, M.A., Briançon, S., Chevalier, Y., 2011. Nanoparticles through the skin: managing conflicting results of inorganic and organic particles in cosmetics and pharmaceutics. Wiley Interdiscip. Rev.: Nanomed. Nanobiotechnol. 3, 463-478.

Cevc, G., Chopra, A., 2016. Deformable (Transfersome®) vesicles for improved drug delivery into and through the skin, Percutaneous Penetration Enhancers Chemical Methods in Penetration Enhancement. Springer, pp. 39-59.

Covi-Schwarz, J., Klang, V., Valenta, C., 2017. ATR-FTIR Spectroscopy and the Skin Barrier: Evaluation of Penetration-Enhancement Effects, in: Dragicevic, N., I. Maibach, H. (Eds.), Percutaneous Penetration Enhancers Drug Penetration Into/Through the Skin: Methodology and General Considerations. Springer Berlin Heidelberg, Berlin, Heidelberg, pp. 247-254.

Deng, P., Teng, F., Zhou, F., Song, Z., Meng, N., Liu, N., Feng, R., 2017. Y-shaped methoxy poly (ethylene glycol)-block-poly (epsilon-caprolactone)-based micelles for skin delivery of ketoconazole: in vitro study and in vivo evaluation. Mater. Sci. Eng. C Mater. Biol. Appl. 78, 296-304.

Dey, S., Rothe, H., Page, L., O'connor, R., Farahmand, S., Toner, F., Marsh, R., Wehmeyer, K., Zhou, S., 2014. An in vitro Skin Penetration Model for Compromised Skin: Estimating Penetration of Polyethylene Glycol [14C]-PEG-7 Phosphate. Skin Pharmacol. Physiol. 28, 12-21.

Döge, N., Avetisyan, A., Hadam, S., Pfannes, E.K.B., Rancan, F., Blume-Peytavi, U., Vogt, A., 2017. Assessment of skin barrier function and biochemical changes of ex vivo human skin in response to physical and chemical barrier disruption. European Journal of Pharmaceutics and Biopharmaceutics 116, 138-148.

Döge, N., Hönzke, S., Schumacher, F., Balzus, B., Colombo, M., Hadam, S., Rancan, F., Blume-Peytavi, U., Schäfer-Korting, M., Schindler, A., Rühl, E., Skov, P.S., Church, M.K., Hedtrich, S., Kleuser, B., Bodmeier, R., Vogt, A., 2016. Ethyl cellulose nanocarriers and nanocrystals differentially deliver dexamethasone into intact, tape-stripped or sodium lauryl sulfate-exposed ex vivo human skin - assessment by intradermal microdialysis and extraction from the different skin layers. J. Controlled Release 242, 25-34.

El Maghraby, G.M., Williams, A.C., Barry, B.W., 2006. Can drug-bearing liposomes penetrate intact skin? J. Pharm. Pharmacol. 58, 415-429.

Elias, P.M., 1983. Epidermal lipids, barrier function, and desquamation. J. Invest. Dermatol. 80, 44s-49s.

Elias, P.M., Steinhoff, M., 2008. "Outside-to-Inside" (and Now Back to "Outside") Pathogenic Mechanisms in Atopic Dermatitis. J. Invest. Dermatol. 128, 1067-1070.

Fernandes, R., Smyth, N.R., Muskens, O.L., Nitti, S., Heuer-Jungemann, A., Ardern-Jones, M.R., Kanaras, A.G., 2015. Interactions of skin with gold nanoparticles of different surface charge, shape, and functionality. Small 11, 713-721.

Gref, R., Miralles, G., Dellacherie, E., 1999. Polyoxyethylene-coated nanospheres: effect of coating on zeta potential and phagocytosis. Polym. Int. 48, 251-256.

Griffiths, C.E., Barker, J.N., 2007. Pathogenesis and clinical features of psoriasis. The Lancet 370, 263-271.

Han, J., Zhu, Z., Qian, H., Wohl, A.R., Beaman, C.J., Hoye, T.R., Macosko, C.W., 2012. A simple confined impingement jets mixer for flash nanoprecipitation. J. Pharm. Sci. 101, 4018-4023.

Harpin, V.A., Rutter, N., 1983. Barrier properties of the newborn infant's skin. J. Pediatr. 102, 419-425.

Hasanovic, A., Winkler, R., Resch, G.P., Valenta, C., 2011. Modification of the conformational skin structure by treatment with liposomal formulations and its correlation to the penetration depth of aciclovir. Eur. J. Pharm. Biopharm. 79, 76-81.

Honeywell-Nguyen, P.L., Gooris, G.S., Bouwstra, J.A., 2004. Quantitative assessment of the transport of elastic and rigid vesicle components and a model drug from these vesicle formulations into human skin in vivo. J. Invest. Dermatol. 123, 902-910.

Hsiao, P.F., Peng, S., Tang, T.-C., Lin, S.-Y., Tsai, H.-C., 2016. Enhancing the in vivo transdermal delivery of gold nanoparticles using poly(ethylene glycol) and its oleylamine conjugate. Int. J. Nanomed. 11, 1867-1878.

Jensen, L.B., Petersson, K., Nielsen, H.M., 2011. In vitro penetration properties of solid lipid nanoparticles in intact and barrier-impaired skin. Eur. J. Pharm. Biopharm. 79, 68-75.

Johnson, B.K., Prud'homme, R.K., 2003. Flash NanoPrecipitation of Organic Actives and Block Copolymers using a Confined Impinging Jets Mixer. Aust. J. Chem. 56, 1021-1024.

Kilfoyle, B.E., Sheihet, L., Zhang, Z., Laohoo, M., Kohn, J., Michniak-Kohn, B.B., 2012. Development of paclitaxel-TyroSpheres for topical skin treatment. J. Controlled Release 163, 18-24.

Knorr, F., Lademann, J., Patzelt, A., Sterry, W., Blume-Peytavi, U., Vogt, A., 2009. Follicular transport route – Research progress and future perspectives. Eur. J. Pharm. Biopharm. 71, 173-180.

Kohli, A.K., Alpar, H.O., 2004. Potential use of nanoparticles for transcutaneous vaccine delivery: effect of particle size and charge. Int. J. Pharm. 275, 13-17.

Labouta, H.I., Schneider, M., 2013. Interaction of inorganic nanoparticles with the skin barrier: current status and critical review. Nanomedicine: Nanotechnology, Biology and Medicine 9, 39-54.

Lalloz, A., Bolzinger, M.-A., Faivre, J., Latreille, P.-L., Garcia Ac, A., Rakotovao, C., Rabanel, J.-M., Hildgen, P., Banquy, X., Briançon, S., 2018. Effect of surface chemistry of polymeric nanoparticles on cutaneous penetration of cholecalciferol. Int. J. Pharm. 553, 120-131.

Lapteva, M., Mondon, K., Moller, M., Gurny, R., Kalia, Y.N., 2014. Polymeric micelle nanocarriers for the cutaneous delivery of tacrolimus: a targeted approach for the treatment of psoriasis. Mol. Pharm. 11, 2989-3001.

Laredj-Bourezg, F., Bolzinger, M.-A., Pelletier, J., Valour, J.-P., Rovère, M.-R., Smatti, B., Chevalier, Y., 2015. Skin delivery by block copolymer nanoparticles (block copolymer micelles). Int. J. Pharm. 496, 1034-1046.

Lifshitz, I.M., Slyozov, V.V., 1961. The kinetics of precipitation from supersaturated solid solutions. J. Phys. Chem. Solids 19, 35-50.

Mahmoud, N.N., Al-Qaoud, K.M., Al-Bakri, A.G., Alkilany, A.M., Khalil, E.A., 2016. Colloidal stability of gold nanorod solution upon exposure to excised human skin: Effect of surface chemistry and protein adsorption. Int. J. Biochem. Cell Biol. 75, 223-231.

Mahmoud, N.N., Alkilany, A.M., Dietrich, D., Karst, U., Al-Bakri, A.G., Khalil, E.A., 2017. Preferential accumulation of gold nanorods into human skin hair follicles: Effect of nanoparticle surface chemistry. J. Colloid Interface Sci. 503, 95-102.

Marukian, N.V., Choate, K.A., 2016. Recent advances in understanding ichthyosis pathogenesis. F1000Res 5, F1000 Faculty Rev-1497.

Moore, T.L., Rodriguez-Lorenzo, L., Hirsch, V., Balog, S., Urban, D., Jud, C., Rothen-Rutishauser, B., Lattuada, M., Petri-Fink, A., 2015. Nanoparticle colloidal stability in cell culture media and impact on cellular interactions. Chem. Soc. Rev. 44, 6287-6305.

OECD, Guidance Document for the Conduct of Skin Absorption Studies. OECD Publishing.

Papakostas, D., Rancan, F., Sterry, W., Blume-Peytavi, U., Vogt, A., 2011. Nanoparticles in dermatology. Arch Dermatol Res 303, 533-550.

Patzelt, A., Richter, H., Knorr, F., Schäfer, U., Lehr, C.-M., Dähne, L., Sterry, W., Lademann, J., 2011. Selective follicular targeting by modification of the particle sizes. J. Controlled Release 150, 45-48.

Paweloszek, R., Briançon, S., Chevalier, Y., Gilon-Delepine, N., Pelletier, J., Bolzinger, M.-A., 2016. Skin Absorption of Anions: Part One. Methodology for In Vitro Cutaneous Absorption Measurements. Pharm. Res. 33, 1564-1575.

Prausnitz, M.R., Langer, R., 2008. Transdermal drug delivery. Nat. Biotechnol. 26, 1261-1268.

Rabanel, J.-M., Faivre, J., Tehrani, S.F., Lalloz, A., Hildgen, P., Banquy, X., 2015a. Effect of the Polymer Architecture on the Structural and Biophysical Properties of PEG–PLA Nanoparticles. ACS Appl. Mater. Interfaces 7, 10374-10385.

Rabanel, J.-M., Faivre, J., Tehrani, S.F., Lalloz, A., Hildgen, P., Banquy, X., 2015b. Effect of the Polymer Architecture on the Structural and Biophysical Properties of PEG–PLA Nanoparticles. ACS Appl. Mater. Interfaces.

Ramezanli, T., Kilfoyle, B.E., Zhang, Z., Michniak-Kohn, B.B., 2017. Polymeric nanospheres for topical delivery of vitamin D3. Int. J. Pharm. 516, 196-203.

Rancan, F., Gao, Q., Graf, C., Troppens, S., Hadam, S., Hackbarth, S., Kembuan, C., Blume-Peytavi, U., Rühl, E., Lademann, J.r., 2012a. Skin penetration and cellular uptake of amorphous silica nanoparticles with variable size, surface functionalization, and colloidal stability. ACS nano 6, 6829-6842.

Rancan, F., Giulbudagian, M., Jurisch, J., Blume-Peytavi, U., Calderón, M., Vogt, A., 2017. Drug delivery across intact and disrupted skin barrier: Identification of cell populations interacting with penetrated thermoresponsive nanogels. European Journal of Pharmaceutics and Biopharmaceutics 116, 4-11.

Rancan, F., Todorova, A., Hadam, S., Papakostas, D., Luciani, E., Graf, C., Gernert, U., Rühl, E., Verrier, B., Sterry, W., Blume-Peytavi, U., Vogt, A., 2012b. Stability of polylactic acid particles and release of fluorochromes upon topical application on human skin explants. Eur. J. Pharm. Biopharm. 80, 76-84.

Shen, H., Hong, S., Prud'homme, R., Liu, Y., 2011. Self-assembling process of flash nanoprecipitation in a multi-inlet vortex mixer to produce drug-loaded polymeric nanoparticles. J. Nanopart. Res. 13, 4109-4120.

Shim, J., Seok Kang, H., Park, W.S., Han, S.H., Kim, J., Chang, I.S., 2004. Transdermal delivery of mixnoxidil with block copolymer nanoparticles. J. Controlled Release 97, 477-484.

Simon, G.A., Maibach, H.I., 2000. The Pig as an Experimental Animal Model of Percutaneous Permeation in Man: Qualitative and Quantitative Observations – An Overview. Skin Pharmacol. Physiol. 13, 229-234.

Soenen, S.J., Parak, W.J., Rejman, J., Manshian, B., 2015. (Intra)Cellular Stability of Inorganic Nanoparticles: Effects on Cytotoxicity, Particle Functionality, and Biomedical Applications. Chem. Rev. 115, 2109-2135.

Štecová, J., Mehnert, W., Blaschke, T., Kleuser, B., Sivaramakrishnan, R., Zouboulis, C.C., Seltmann, H., Korting, H.C., Kramer, K.D., Schäfer-Korting, M., 2007. Cyproterone Acetate Loading to Lipid Nanoparticles for Topical Acne Treatment: Particle Characterisation and Skin Uptake. Pharm. Res. 24, 991-1000.

Tak, Y.K., Pal, S., Naoghare, P.K., Rangasamy, S., Song, J.M., 2015. Shape-Dependent Skin Penetration of Silver Nanoparticles: Does It Really Matter? Sci. Rep. 5.

Tsai, J.-C., Shen, L.-C., Sheu, H.-M., Lu, C.-C., 2003. Tape stripping and sodium dodecyl sulfate treatment increase the molecular weight cutoff of polyethylene glycol penetration across murine skin. Arch. Dermatol. Res. 295, 169-174.

Tsai, J.-C., Sheu, H.-M., Hung, P.-L., Cheng, C.-L., 2001. Effect of barrier disruption by acetone treatment on the permeability of compounds with various lipophilicities: Implications for the permeability of compromised skin. J. Pharm. Sci. 90, 1242-1254.

Vogt, A., Combadiere, B., Hadam, S., Stieler, K.M., Lademann, J., Schaefer, H., Autran, B., Sterry, W., Blume-Peytavi, U., 2006. 40[thinsp]nm, but not 750 or 1,500[thinsp]nm, Nanoparticles Enter Epidermal CD1a+ Cells after Transcutaneous Application on Human Skin. J. Invest. Dermatol. 126, 1316-1322.

Wagner, C., 1961. Theorie der alterung von niederschlägen durch umlösen (Ostwald-reifung). Berichte der Bunsengesellschaft für physikalische Chemie 65, 581-591.

Wooster, T.J., Golding, M., Sanguansri, P., 2008. Impact of Oil Type on Nanoemulsion Formation and Ostwald Ripening Stability. Langmuir 24, 12758-12765.

Wu, X., Landfester, K., Musyanovych, A., Guy, R.H., 2010. Disposition of Charged Nanoparticles after Their Topical Application to the Skin. Skin Pharmacol. Physiol. 23, 117-123.

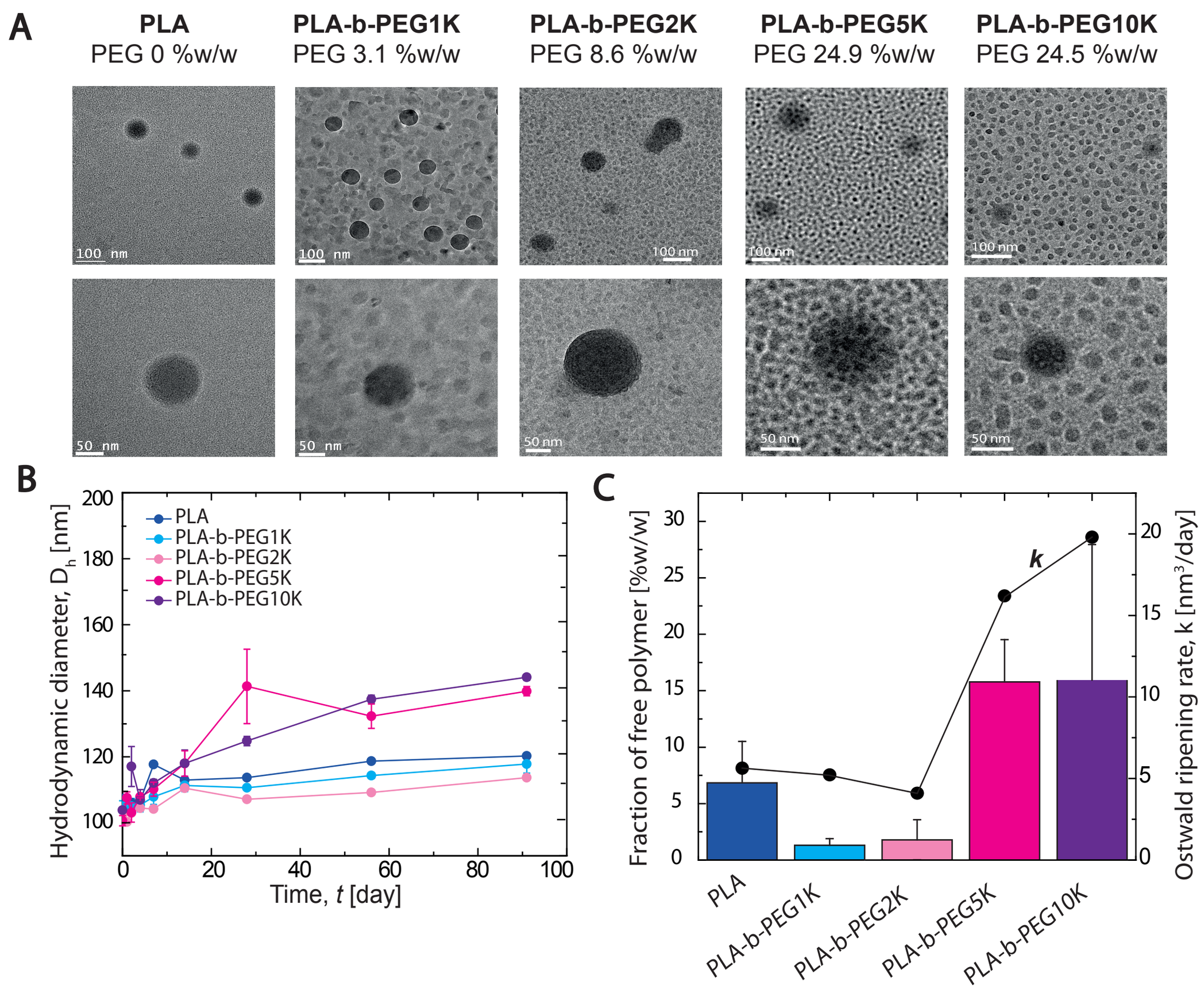
A
PLA
PEG 0 %w/w
PLA-b-PEG1K
PEG 3.1 %w/w
PLA-b-PEG2K
PEG 8.6 %w/w
PLA-b-PEG5K
PEG 24.9 %w/w
PLA-b-PEG10K
PEG 24.5 %w/w
100 nm
50 nm
B
Hydrodynamic diameter, $D_h$ [nm]
Time, t [day]
PLA
PLA-b-PEG1K
PLA-b-PEG2K
PLA-b-PEG5K
PLA-b-PEG10K
C
Fraction of free polymer [%w/w]
Ostwald ripening rate, k [nm³/day]
k
PLA
PLA-b-PEG1K
PLA-b-PEG2K
PLA-b-PEG5K
PLA-b-PEG10K

A

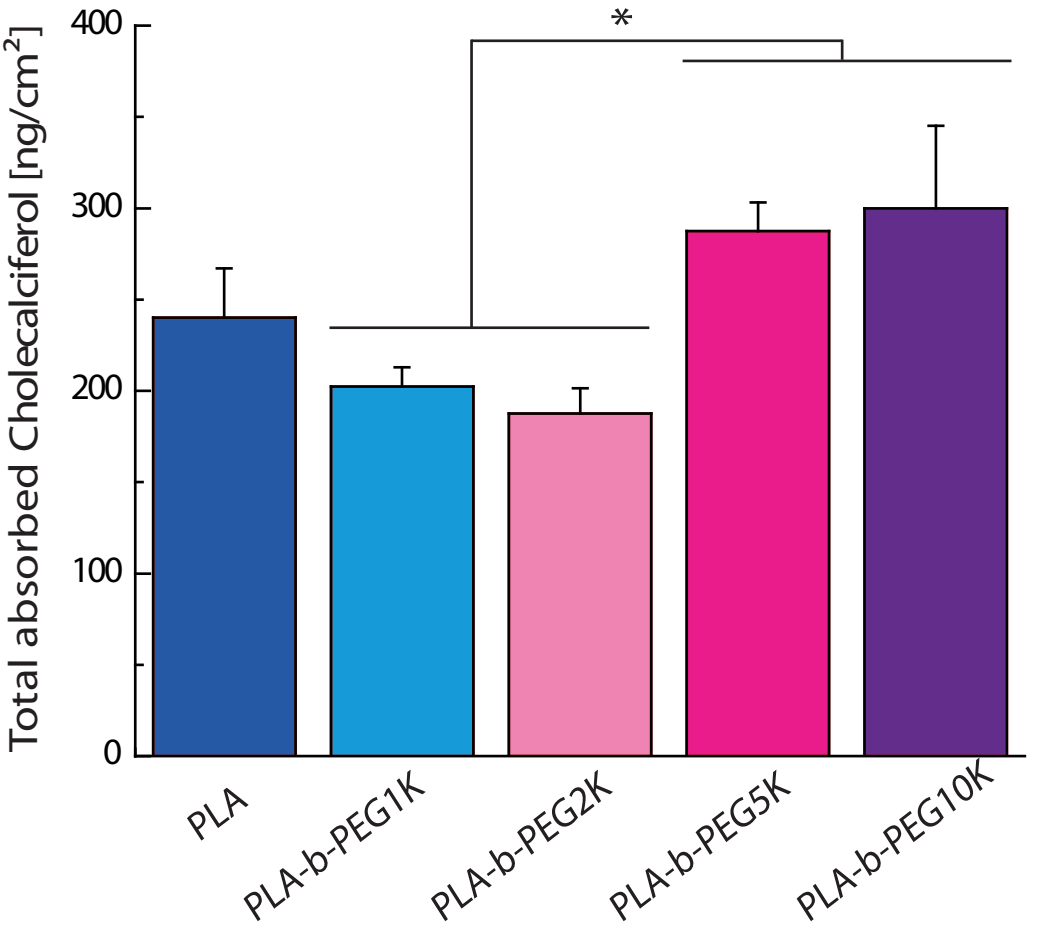
Total absorbed Cholecalciferol [ng/cm²]
400
300
200
100
0
*
PLA
PLA-b-PEG1K
PLA-b-PEG2K
PLA-b-PEG5K
PLA-b-PEG10K

B

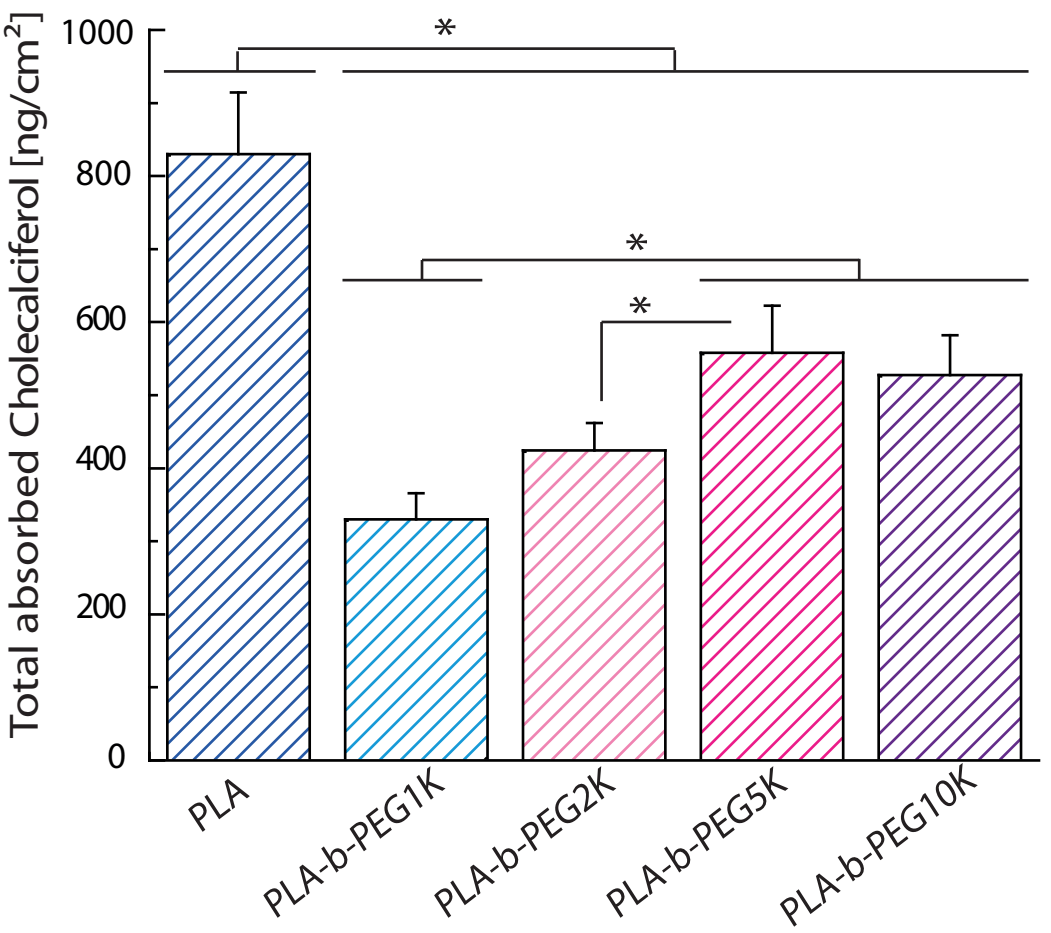
Total absorbed Cholecalciferol [ng/cm²]
1000
800
600
400
200
0
*
*
*
PLA
PLA-b-PEG1K
PLA-b-PEG2K
PLA-b-PEG5K
PLA-b-PEG10K

C

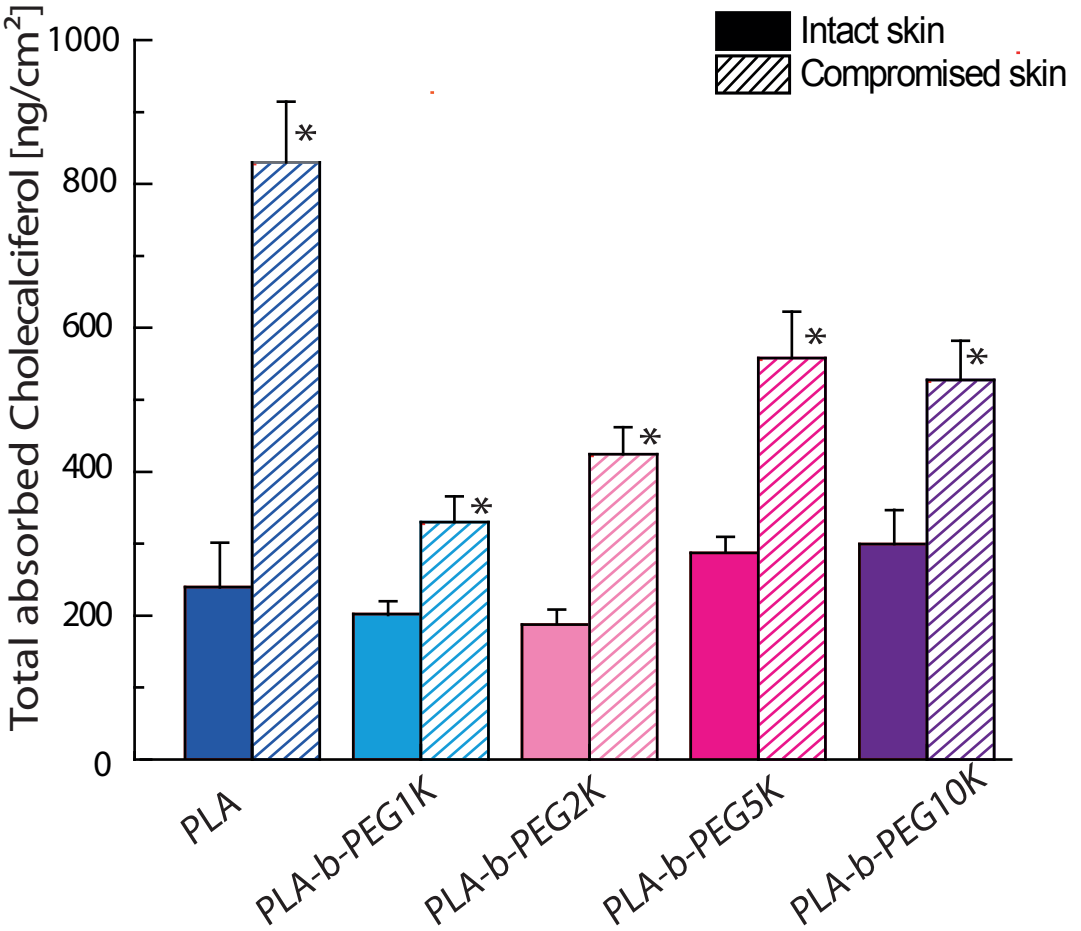
Intact skin
Compromised skin
Total absorbed Cholecalciferol [ng/cm²]
1000
800
600
400
200
0
*
*
*
*
*
PLA
PLA-b-PEG1K
PLA-b-PEG2K
PLA-b-PEG5K
PLA-b-PEG10K

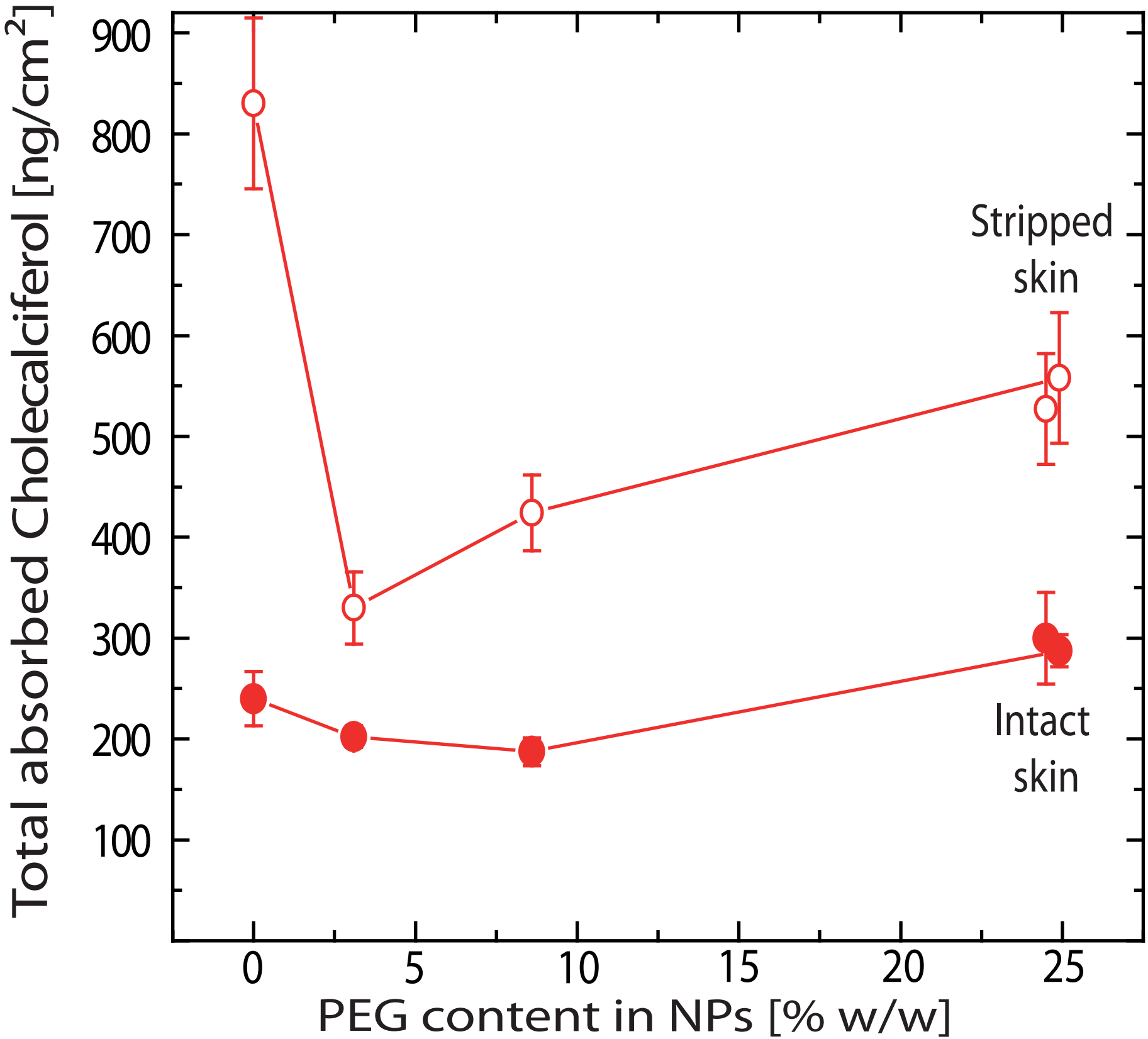
Total absorbed Cholecalciferol [ng/cm$^2$]
900
800
700
600
500
400
300
200
100
0
5
10
15
20
25
PEG content in NPs [% w/w]
Stripped skin
Intact skin

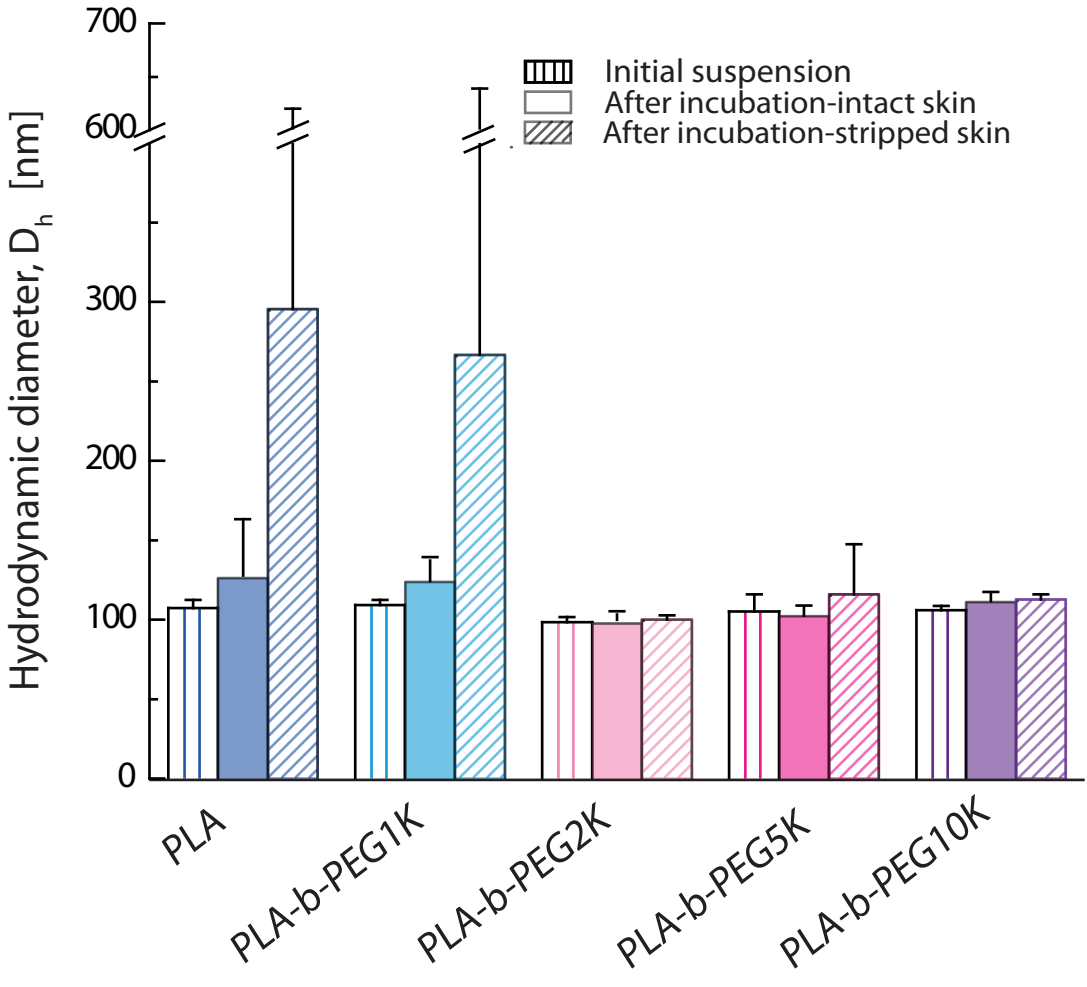
Hydrodynamic diameter, $D_h$ [nm]
700
600
300
200
100
0
Initial suspension
After incubation-intact skin
After incubation-stripped skin
PLA
PLA-b-PEG1K
PLA-b-PEG2K
PLA-b-PEG5K
PLA-b-PEG10K

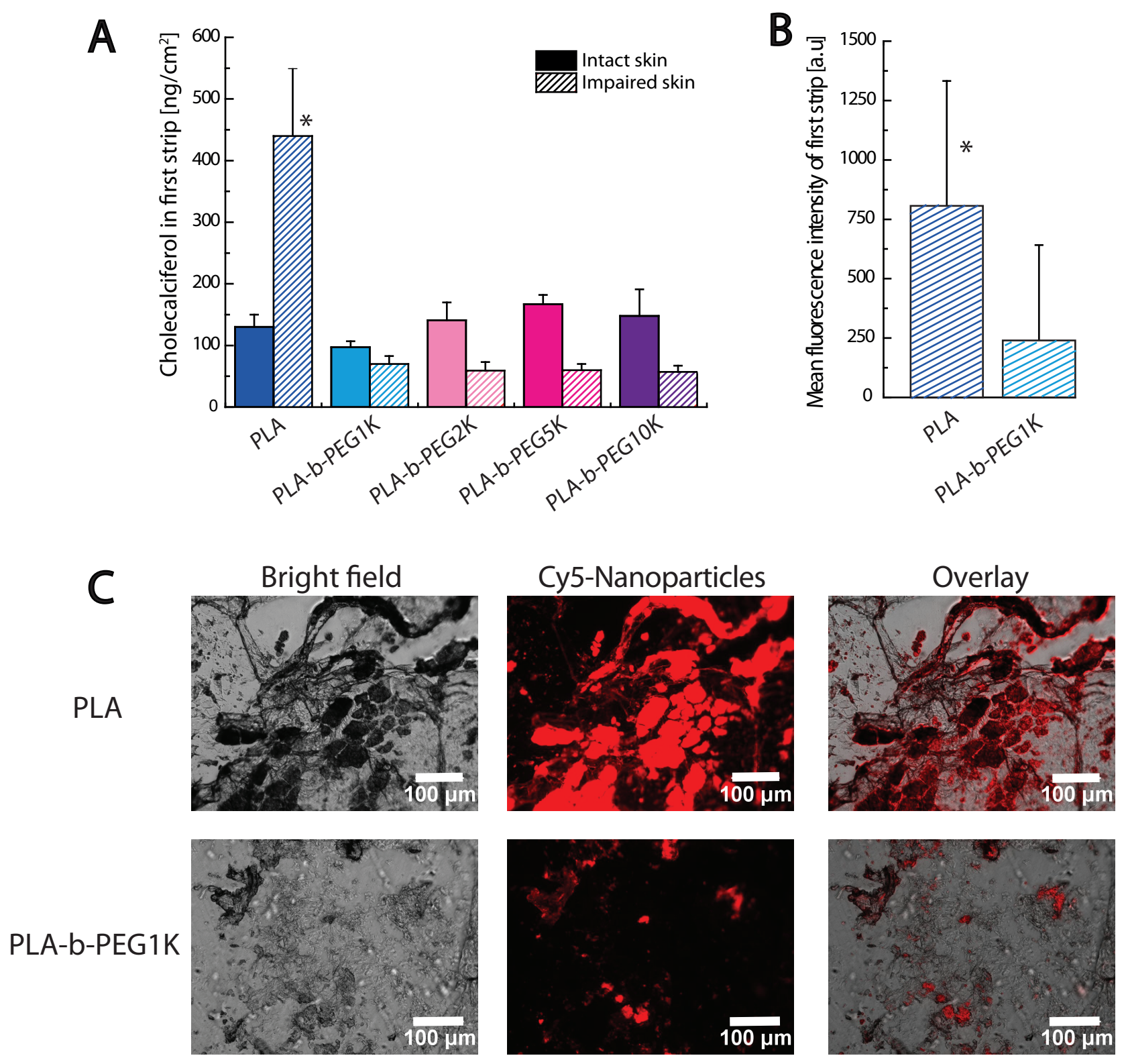
A
Cholecalciferol in first strip [ng/cm²]
600
500
400
300
200
100
0
Intact skin
Impaired skin
*
PLA
PLA-b-PEG1K
PLA-b-PEG2K
PLA-b-PEG5K
PLA-b-PEG10K
B
Mean fluorescence intensity of first strip [a.u]
1500
1250
1000
750
500
250
0
*
PLA
PLA-b-PEG1K
C
Bright field
Cy5-Nanoparticles
Overlay
PLA
PLA-b-PEG1K
100 µm

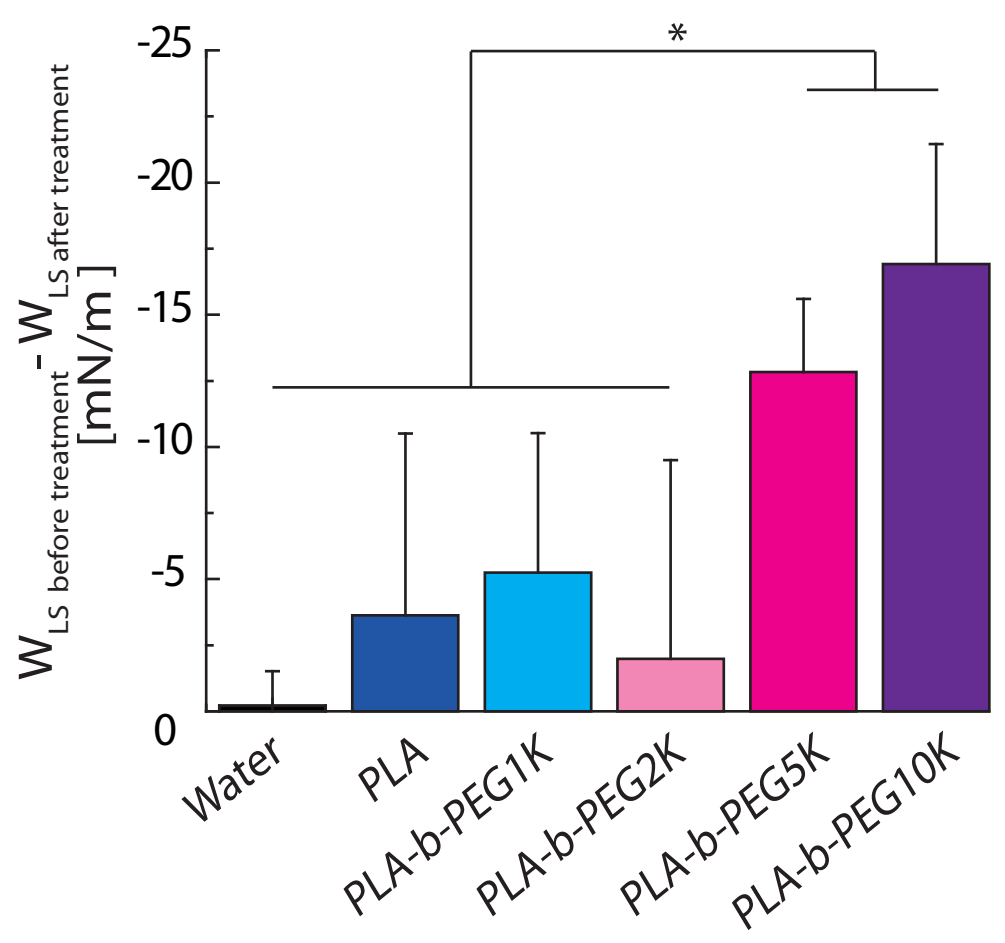
*
-25
-20
-15
-10
-5
0
$W_{LS\ before\ treatment} - W_{LS\ after\ treatment}$ [mN/m]
Water
PLA
PLA-b-PEG1K
PLA-b-PEG2K
PLA-b-PEG5K
PLA-b-PEG10K

***Table 1.*** *Polymer characteristics*

| **Polymer** | ***PEG chain size*** | ***Total Mn* (GPC)** | ***Total Mw* (GPC)** | ***Total Mw* (NMR) *** | **PdI (GPC) **** | ***PLA chain size ****** | **PEG content (NMR) ******** |
|---|---|---|---|---|---|---|---|
| | *[g/mol]* | *[g/mol]* | *[g/mol]* | *[g/mol]* | | *[g/mol]* | *[%w/w$_{total}$]* |
| PLA | - | 26 700 | 36 300 | ND | 1.4 | 36300 | - |
| PLA-Cy5 | - | 26 700 | 36 300 | ND | 1.4 | 36300 | - |
| PLA-*b*-PEG1K | 1 000 | 18 200 | 26 500 | 32 300 | 1.5 | 25500 | 3.1 |
| PLA-*b*-PEG2K | 2 000 | 14 600 | 22 300 | 23 300 | 1.5 | 20300 | 8.6 |
| PLA-*b*-PEG5K | 5 000 | 14 700 | 19 140 | 20 100 | 1.3 | 14140 | 24.9 |
| PLA-*b*-PEG10K | 10 000 | 20 100 | 27 900 | 40 800 | 1.4 | 17900 | 24.5 |

* calculated from the number of LA residues per PEG chain given by the integration of peak intensity ratios of PEG (3.6 ppm) and PLA (5.2 ppm) by $^{1}$H NMR

** calculated from the GPC analysis: PdI=*Mw/Mn*

*** calculated as follow: PLA size (GPC) =Total PLA-*b*-PEG *Mw* (GPC)−PEG size

**** calculated from the $^{1}$H NMR results: $PEG\%w/w = \frac{Mw\ PEG}{(Mw\ PEG + Mw\ PLA\ chain)} \times 100$

***Table 2***. *Physico-chemical characteristics of NPs. Data are reported as mean over three separate formulations ± SD*

| **Polymer** | **PLA** | **PLA-*b*-PEG1K** | **PLA-*b*-PEG2K** | **PLA-*b*-PEG5K** | **PLA-*b*-PEG10K** |
|---|---|---|---|---|---|
| % PEG in polymer | 0 | 3.1 | 8.6 | 24.9 | 24.5 |
| Z-average size [nm] | 100 ±3 | 103 ±3 | 104±2 | 102±6 | 102±1 |
| Number mean size [nm] | 73±6 | 74±3 | 72±6 | 69±2 | 70±2 |
| PdI | 0.09±0.01 | 0.07±0.02 | 0.1±0.03 | 0.1±0.01 | 0.09±0.01 |
| Zeta potential [mV] | -33±2 | -23±2 | -13±2 | -6±1 | -3.5±0.2 |
| Drug loading [%w/w] | 7.3 ±0.2 | 7.2±0.3 | 7.3±0.2 | 6.7±0.3 | 7.5±0.1 |
| Drug yield [%] | 95±2 | 96±2 | 98±1 | 97±1 | 98±3 |
| PEG surface density [ethylene glycol units/nm$^2$] | - | 3±1 | 15±2 | 48±6 | 41±5 |

***Table 3.*** *Effects of formulation type on cholecalciferol distribution in skin layers in intact and impaired pig skin after 24 h exposure. Applied dose was 35 µg/cm$^2$. Data are given as mean ± SEM.*

| | PLA NPs (ng.cm$^{-2}$) | | PLA-b-PEG1K NPs (ng.cm$^{-2}$) | | PLA-b-PEG2K NPs (ng.cm$^{-2}$) | | PLA-b-PEG5K NPs (ng.cm$^{-2}$) | | PLA-b-PEG10K NPs (ng.cm$^{-2}$) | |
|---|---|---|---|---|---|---|---|---|---|---|
| | *Intact skin* | *Stripped skin* | *Intact skin* | *Stripped skin* | *Intact skin* | *Stripped skin* | *Intact skin* | *Stripped skin* | *Intact skin* | *Stripped skin* |
| *SC* | 132 ±16 | - | 99 ±12 | - | 109 ±16 | - | 163 ±12 | - | 196 ±31 | - |
| *VE* | 80 ±15 | 567 ±72 | 78 ±11 | 218 ±31 | 58 ±9 | 326 ±29 | 100 ±14 | 426 ±61 | 78 ±14 | 382 ±76 |
| *D* | 25 ±2 | 258 ±41 | 22 ±1 | 126 ±19 | 16 ±1 | 92 ±17 | 20 ±5 | 127 ±32 | 19 ±3 | 142 ±41 |
| *Total* | 237 ±26 | 823 ±86 | 200 ±11 | 344 ±35 | 183 ±14 | 418 ±37 | 283 ±17 | 552 ±56 | 295 ±43 | 525 ±57 |

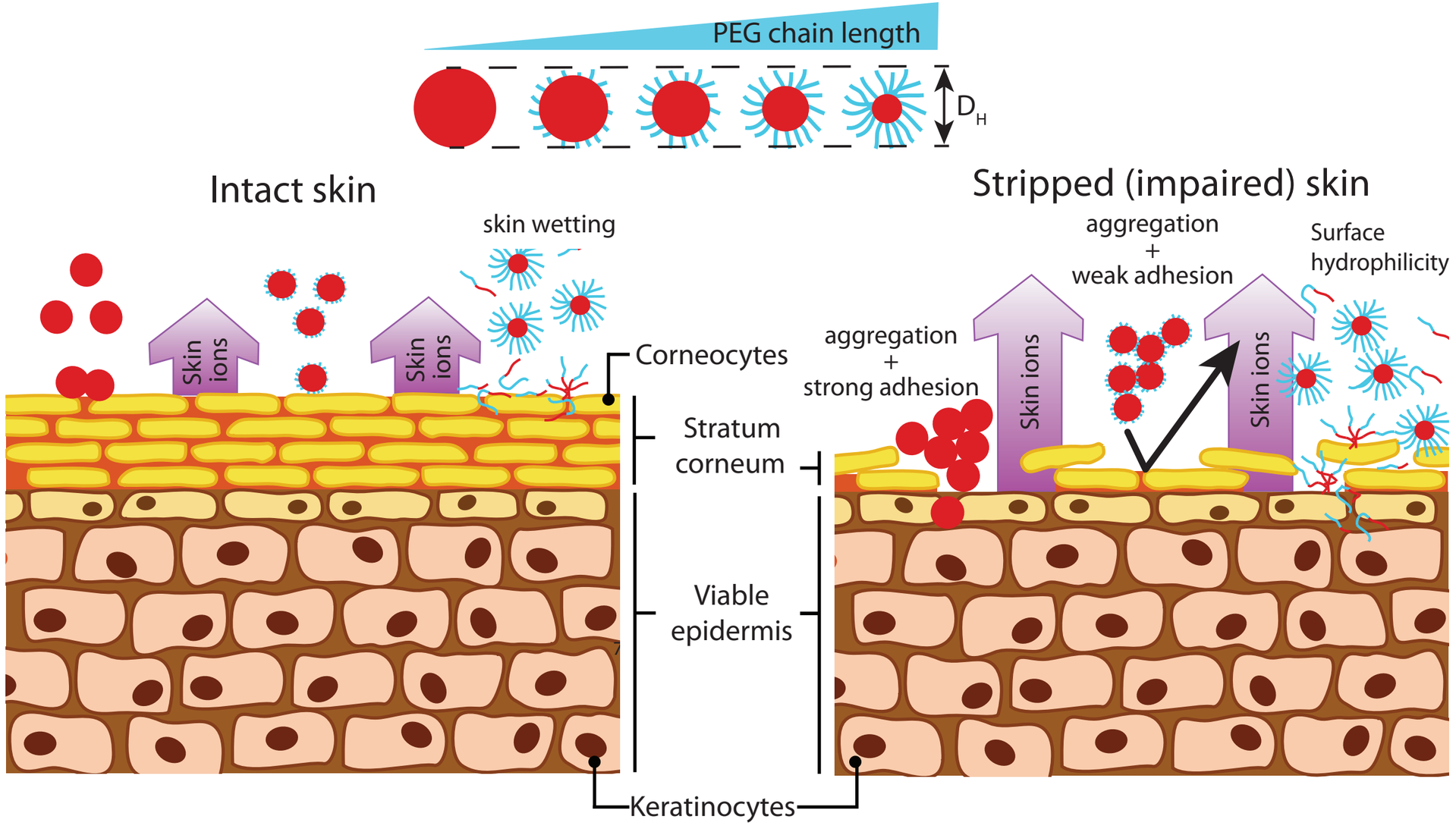
PEG chain length
$D_H$
Intact skin
skin wetting
Skin ions
Skin ions
Corneocytes
Stratum corneum
Viable epidermis
Keratinocytes
Stripped (impaired) skin
aggregation + weak adhesion
Surface hydrophilicity
aggregation + strong adhesion
Skin ions
Skin ions